UCLouvain

AGRO LOUVAIN

Faculté des bioingénieurs

Assessing the Response of Seychelles Fish Biodiversity to Protection Status and Seascape Conditions

Author : JACQUEMIN Marie
Supervisors : HANERT Emmanuel, DOBBELAERE Thomas
Readers : HARLAY Jérôme, DELEERSNIJDER Eric
Academic year 2023-2024
Thesis presented in partial fulfilment of the requirements for the degree of Master of Bioengineering : Environmental Bioengineering

Abstract

Marine protected areas (MPAs) are a common tool used worldwide to enhance the protection of marine biodiversity. In recent years, MPAs and MPA networks have begun to include the question of connectivity, which manifests through the movement of juveniles and adults, in their creation with the goal to enhance population stability and diversity in and out of MPAs. In this study, we investigate the connectivity of the current MPA network located on the Mahé Plateau, Seychelles with the goal to identify the dispersal dynamic of fish larvae and potential gaps in the network. To do so, we use a three-dimensional ocean model, SLIM3D, over a seven-month period. We couple it with a larval dispersal model based on the behaviour of Lutjanus sebae, a key commercial and overexploited fish in the Seychelles. Larvae behaviour is divided into five main life stages: egg, pre-flexion, flexion, post-flexion and settlement. We then conduct a connectivity analysis on the MPAs and reefs located on the Mahé plateau. Our results suggest that the varying dynamic of the currents has an impact on the direction of exchanges of larvae between the inner islands and outer reefs of the plateau as well as on the percentage of settling larvae which reaches a peak in January (12.5%). We find that the probability of exchange between MPAs currently reach up to 2.8% and identify potential locations of new MPAs on reefs with a high potential of exporting and receiving larvae around Mahé island.

Acknowledgements

Many people have participated directly and indirectly in the realization of this thesis.

Firstly, I thank my supervisor, Emmanuel Hanert who has provided his guidance and been available through the entire year, in and out of our weekly meetings.

I thank my co-supervisor, Thomas Dobbelaere without whom this thesis would never have been completed and who helped me through so many problems I encountered.

I thank Jérôme Harlay and Eric Deleersnijder for accepting and taking the time to read this thesis. I additionally thank Jérôme Harlay for offering his help and time during our different meetings.

I thank the entire SLIM team —Riana, Lauranne, Douchan, Alexis, and Amaury— who were present every Friday to offer their advice and support.

I would like to thank every person who has provided much-needed data : Amanda Port-Louis who provided the Marine Protected Areas of the Seychelles Marine Spatial Plan as well as Vincent Amelie and Beryl Andrade, from the Seychelles MetOffice, who provided wind velocity measurements recorded at the Seychelles Airport.

I also thank my teammates, Julien, Mattias and Louis with whom I shared so many coffee and puzzle breaks and who have become cherished friends.

Finally, I would like to thank my friends —Tracy, Clara, Robin, Inessa and Hélios— who have brought me so much support and joy throughout this year as well as my family who has pushed me forward even during hard times.

Table of Contents

Acronyms

ACA Allen Coral Atlas
ADCP Acoustic Doppler current profiler
EEZ Exclusive Economic Zone
GEBCO General Bathymetric Chart of the Oceans
ID In-degree
IPCC Intergovernmental Panel on Climate Change
IUCN International Union for Conservation of Nature
LR Local retention
LPT Lagrangian Particle Tracker
MP Mahé plateau
MPA Marine Protected Area
MPAn Marine Protected Area Network
NEMO Nucleus for European Modelling of the Ocean
OD Out-degree
PA Protected Area
PLD Pelagic larval duration
RMSE root mean square error.
SLIM Second-generation Louvain-la-Neuve Ice-ocean Model
SLOMO Seychelles Local Ocean Modeling and Observation program
SR Self-recruitment
WCL Weighted connectivity length
WINDS Western INDian Ocean Simulation

1. Introduction

1.1 Consequences of climate change on marine ecosystems

Humanity relies on the services provided by the Earth's ecosystems to support its well-being, from the most basic needs like food and water to its cultural development (Ecosystems and Human Well-Being: Biodiversity Synthesis 2005). Marine ecosystems, in particular, have produced 177.8 metric tons of aquatic animals, mostly intended for human consumption, through fisheries and aquaculture in 2020. Nowadays, the livelihoods of an estimated 600 million people depend, at least partially, on fisheries and aquaculture. (FAO 2022).

The negative effects caused by the pressure of human activities on those marine ecosystems has been well documented. Overfishing and marine pollution are responsible for the destruction of marine habitats and the loss of biodiversity, especially in the deep ocean (Coleman and Williams 2002). Human activities have also been shown to have an impact on the concentration of greenhouse gases (CO2, CH4, N2O…) in the atmosphere causing a general warming of the Earth's surface and impacting both terrestrial and marine ecosystems (Fig. 1). Climate change has had two main impacts on the state of the ocean, firstly leading to a global increase of the ocean surface temperature which reached 0.88°C between 1850-1900 and 2011-2020 (Calvin et al. 2023) and, secondly, causing the acidification of the surface layers of the ocean which acts as a sink for anthropogenic CO2 and absorbs around 30% of its emissions (Gruber et al. 2019).

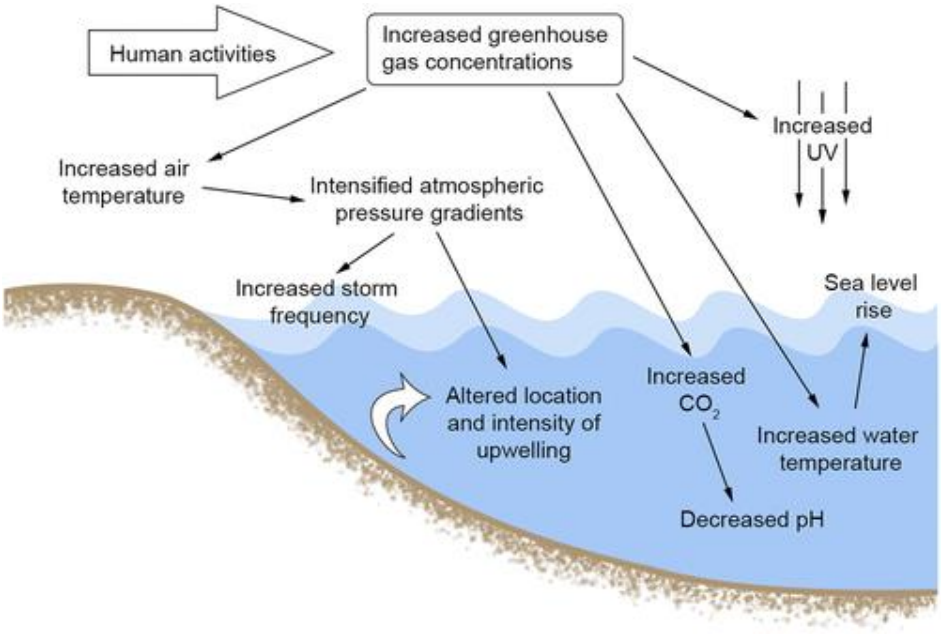

Figure 1 Main impacts of climate change on marine environments (Harley et al. 2006)

The changes in ocean conditions caused by this rise in temperature are predicted to have an impact on the distribution of fish species and lead to local extinctions (Cheung et al. 2009; Pinsky et al. 2013) and even to a decrease in fish body weight (Cheung et al. 2013). Those distributional and productivity changes could in turn negatively impact the production of fisheries (Lam et al. 2016).

The impacts of acidification on marine organisms are difficult to quantify as the response can vary between taxonomic groups. However, there seems to be a global decrease in the survival, growth, development and abundance in a broad range of marine species (Kroeker et al. 2013) and an negative impact on a large range of shell building organisms (Doney et al. 2009; Guinotte and Fabry 2008).

Vegetated coastal habitats (seagrass meadows, mangroves, and salt marshes) are also threatened by different stressors such as aquaculture, global warming and physical disturbances. They play an important role as habitat and food source for commercial fishery species as well as megaherbivores like green sea turtles (Orth et al. 2006). Furthermore, those habitats, while covering less than 0.5% of the seabed, account for 50 to 71% of carbon storage in ocean sediments (Nellemann and GRID--Arendal 2009) giving them the name of 'blue carbon sinks'. This carbon storage happens through the sedimentation of algal detritus reaching the seabed where it can remain for decades (Heck et al. 2008). 2 to 7% of blue carbon sinks are currently being lost every year (Nellemann and GRID--Arendal 2009).

1.2 Marine protected areas

As a consequence of the effects of climate change, it appears necessary to, not only limit the emissions of greenhouse gases, but also to implement new ways to protect the Earth's ecosystem. A common tool to hamper the loss of biodiversity, let it be in terrestrial and marine ecosystems, are protected areas. The general concept of protected areas is not a recent one and can go back to the nineteenth century. However, those areas were originally used to protect locations considered as "feats of nature" and of little importance to the economy. It was not until the 1970s that the question of biodiversity conservation and environment degradation became a concern for their creation (Fig. 2) (Dudley and Stolton 2008; Watson et al. 2014).

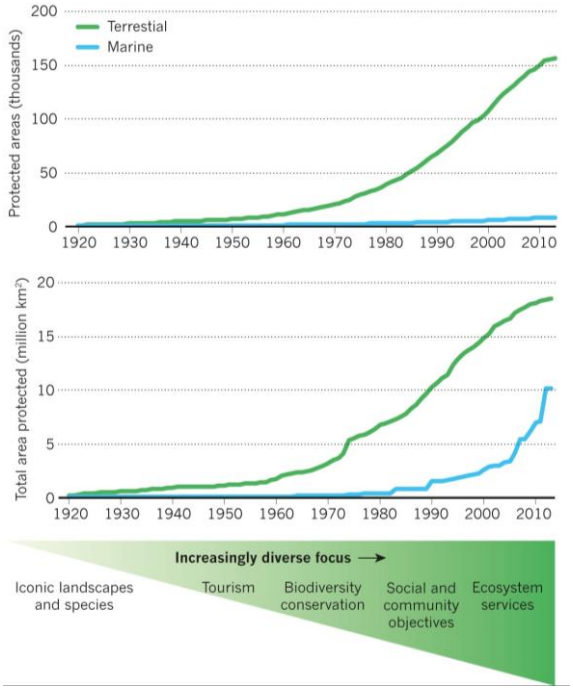

Figure 2 Growth of the modern terrestrial and marine protected area estate (Watson et al. 2014)

Marine Protected Areas (MPAs), specifically, can be defined as 'areas that afford some level of special protection to parts of the ocean of conservation purposes' (Connell and Gillanders 2007). This definition, however, allows for a wide variation in protection and management of MPAs. The MPA guide established in 2021, as complement to the IUCN Protected Area Categories, divides MPAs in four categories, from minimally to fully protected (Fig. 3) (Grorud-Colvert et al. 2021).

Figure 3 Level of protection based on maximum allowed impact of seven potential activities in MPAs (Grorud-Colvert et al. 2021)

MPAs have shown, to have a positive impact on the conservation and recovery of marine species (eg. (Speed, Cappo, and Meekan 2018)). However, numerous factors, biological and socio-economic, can influence the response of targeted and non-targeted species making their effects uncertain even years after their creation (Babcock et al. 2010). Their efficiency is, for example, highly dependent on their design and management; five key characteristics have been recognized to improve greatly their conservation benefits : (1) a no take policy, no fish or plant can be removed from the protected area, (2) good enforcement, (3) being older than 10 years old, (4) being larger than 100 km2, (5) isolation by deep sand or water (Edgar et al. 2014). Their management, after their creation, should also not be overlooked : the budget allocated and the staff capacity (Gill et al. 2017) as well as the local socioeconomic conditions (McClanahan et al. 2006) can become constraints in their well-development.

The preoccupations leading the creation of PAs and MPAs have thus gradually changed over time and now have to accommodate for the impacts of climate change which, in the case of MPAs, include increasing temperature, sea-level rise and ocean acidification in addition to previously known threats such as overfishing.

When well-managed, MPAs can help climate change adaptation through different ways. MPAs help protect wetlands (mangroves, seagrasses and salt marshes) which can in turn offer a safe habitat to different species as well as maintain carbon sequestration. They also enhance the reproduction of populations making them more resistant to extinction and prevent biodiversity loss by diminishing stressors caused by human activities. MPAs can also provide refugia for species migrating because of a change in salinity or temperature (Roberts et al. 2017) as well as promote genetic diversity within species allowing for a better adaption and evolution to the impacts of climate change (Carr et al. 2017).

1.3 Connectivity

In its most general sense, connectivity refers to the processes that determine the connections between populations, species, communities or ecosystems. More precisely, ecological spatial connectivity refers to ‘the processes by which genes, organisms, populations, species, nutrients, and/or energy move among spatially distinct habitats, populations, communities, or ecosystems’ (Carr et al. 2017).

Ecological spatial connectivity can be divided into four categories defined by Carr et al. (2017) : (1) Population connectivity, the movement of individuals of a single species among patchily distributed local or subpopulations which may be separated because of unhabitable areas. Those movements influence the number of individuals as well as the structure of the local population. (2) Genetic connectivity, the movement of genes and their impacts on evolutionary processes within subpopulations of a single species. (3) Community connectivity, the movement of multiple species among distinct ecological communities formed by species that interact in particular habitats. (4) Ecosystem connectivity, the movement of multiple species, chemicals, materials and energy in the form of organisms (Carr et al. 2017; Lowe and Allendorf 2010).

Population connectivity can be studied through the exchange of eggs, larvae recruits or other propagules, juveniles or adults that happen within subpopulations of a single species (Palumbi 2003). This exchange can happen through passive dispersal (in the case of fish larvae, eggs and spores carried by water currents) or active migrations (in the case of adult and juveniles organisms) (Berkström, Wennerström, and Bergström 2022). The distance crossed through passive dispersal varies from species to species : fishes and invertebrates with a pelagic larval phase are able to disperse over long distances ranging from tens to hundreds of kilometers (Kinlan and Gaines 2003), whereas macrophytes might need to attach to floating objects to do so and travel smaller distances (Fig. 4) (Winston 2012).

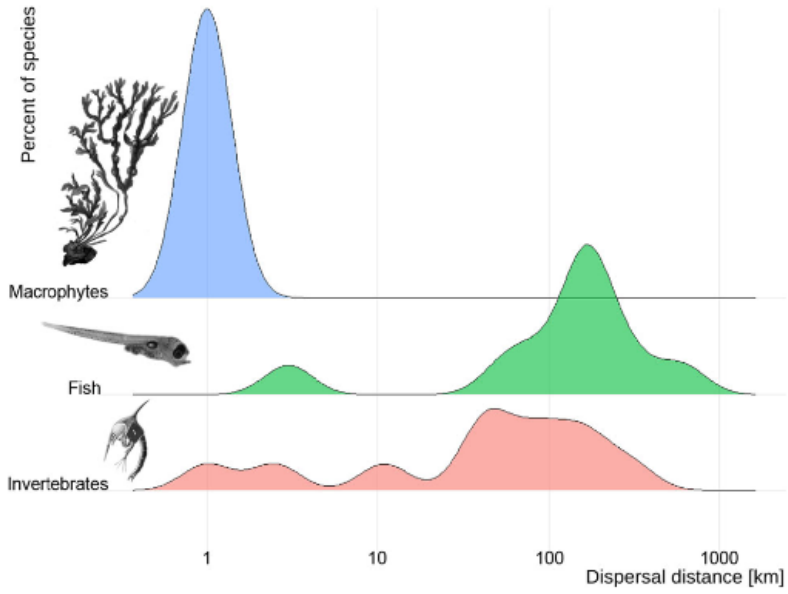

Figure 4 Dispersal distances for spores and pelagic larvae from macropyhytes, invertebrates and fishes in the Baltic Sea, Kattegat and Skagerrak. (Berkström, Wennerström, and Bergström 2022) adapted from (Kinlan and Gaines 2003)

In the context of MPAs, connectivity manifests through the movement of juveniles and adults from and to areas outside and inside of MPAs. Parts of MPAs rely on the arrival of populations spawned outside of the MPA and others act as a source of populations for areas outside the MPA. Those movements can in turn increase the stability, size and diversity of populations inside the protected sites and in the surrounding waters.

To include connectivity into their creation and management, MPAs have to be considered as MPA networks: "an organized collection of individual MPAs operating co-operatively and synergistically, at various spatial scales and with a range of protection levels, to fulfill ecological aims more effectively and comprehensively than individual sites could alone" (Laffoley 2008). In a network, MPAs would need to function collectively to reach biodiversity goals with connectivity being only one aspect of the MPA network creation. The IUCN-WCPA sets five guidelines to ensure the creation of an effective MPA network including connectivity (ecological linkages): (1) Include the full range of biodiversity present in the biogeographic region. (2) Ensure ecologically significant areas are incorporated. (3) Maintain long-term protection. (4) Ensure ecological linkages. (5) Ensure maximum contribution of individual MPAs to the network. (Laffoley 2008)

In spite of its advantages, connectivity is still an overlooked process in the creation and study of MPAs. A 2018 study showed that, among five countries with advanced marine spatial planning (namely France, Australia, the UK, the US and Canada) , only 11% of the MPAs considered connectivity as an ecological criterion (Balbar and Metaxas 2019). Software tools such as MARXAN (Ball, Possingham, and Watts 2009), which identifies optimal PA and MPA networks for the lowest socio-economic cost, are more commonly used during the planning process (Airamé et al. 2003; Green et al. 2009). MARXAN has more recently implemented the use of previously established connectivity data (dispersal model, genetics…) to establish and include connectivity metrics in its calculations through Marxan Connect (Daigle et al. 2020).

1.4 The Seychelles archipelago

The Seychelles archipelago is located in the Western Indian Ocean, north of Madagascar (Fig. 5). It consists of 155 islands with most of its population (98-99%) living on the central islands of the Mahé plateau, a shallow plateau of around 40 000 km^2 located in the north-eastern part of the archipelago (GOS 2014).

The Seychelles Exclusive economic zone (EEZ) (Fig. 5), the area where it has jurisdiction over natural resources (fish, offshore oil and gas) (Hannesson 2013), is one of the 25 largest in the world. and its biodiversity is at the base of its economy, supporting tourism, fisheries and local livelihoods (Seychelles Marine Spatial Plan Initiative 2023).

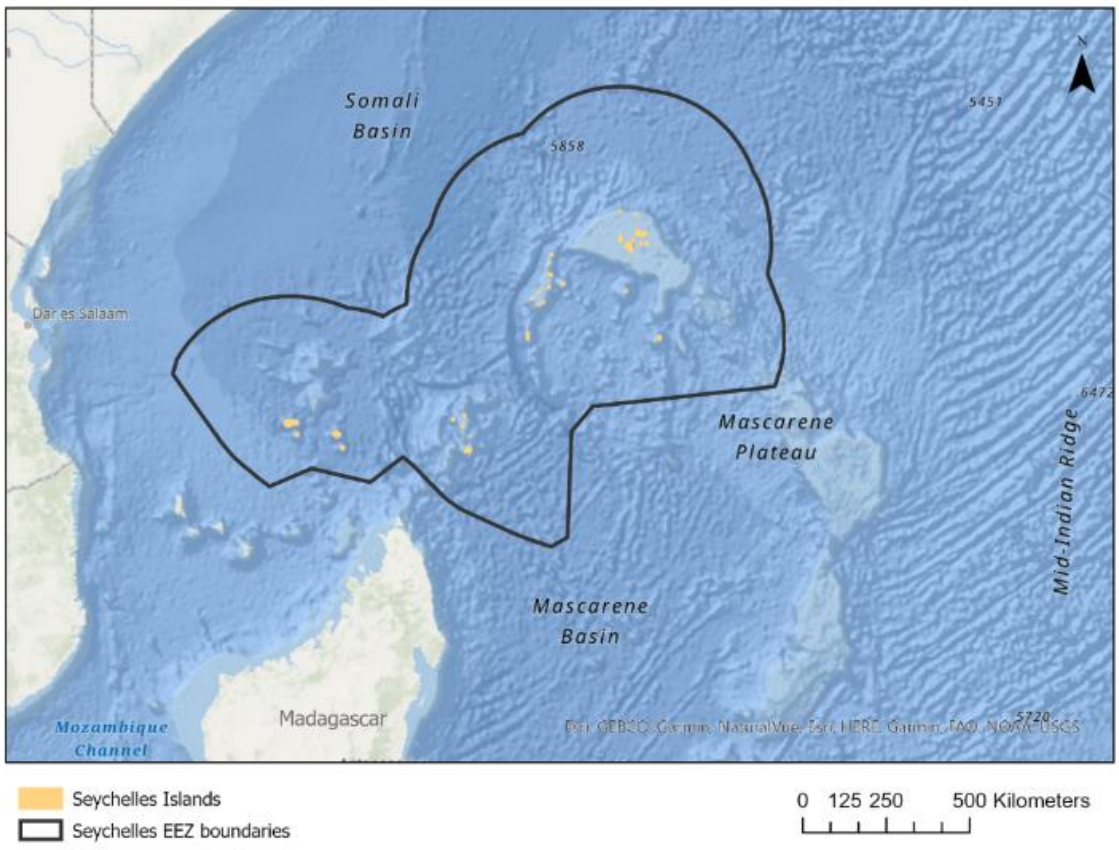

Figure 5 Location and limits of the Seychelle's Exclusive Economic Zone

Following a six year plan set in motion in 2014 , the Seychelles has protected 30% of its EEZ with MPAs (Fig. 6). Half of those areas are of high biodiversity protection where almost no human activity is permitted. The other half is of medium biodiversity protection and sustainable use, allowing for activities necessary to the Seychelles' economy under regulations. (Seychelles Designates 30% of its EEZ as Marine Protected Area 2020).

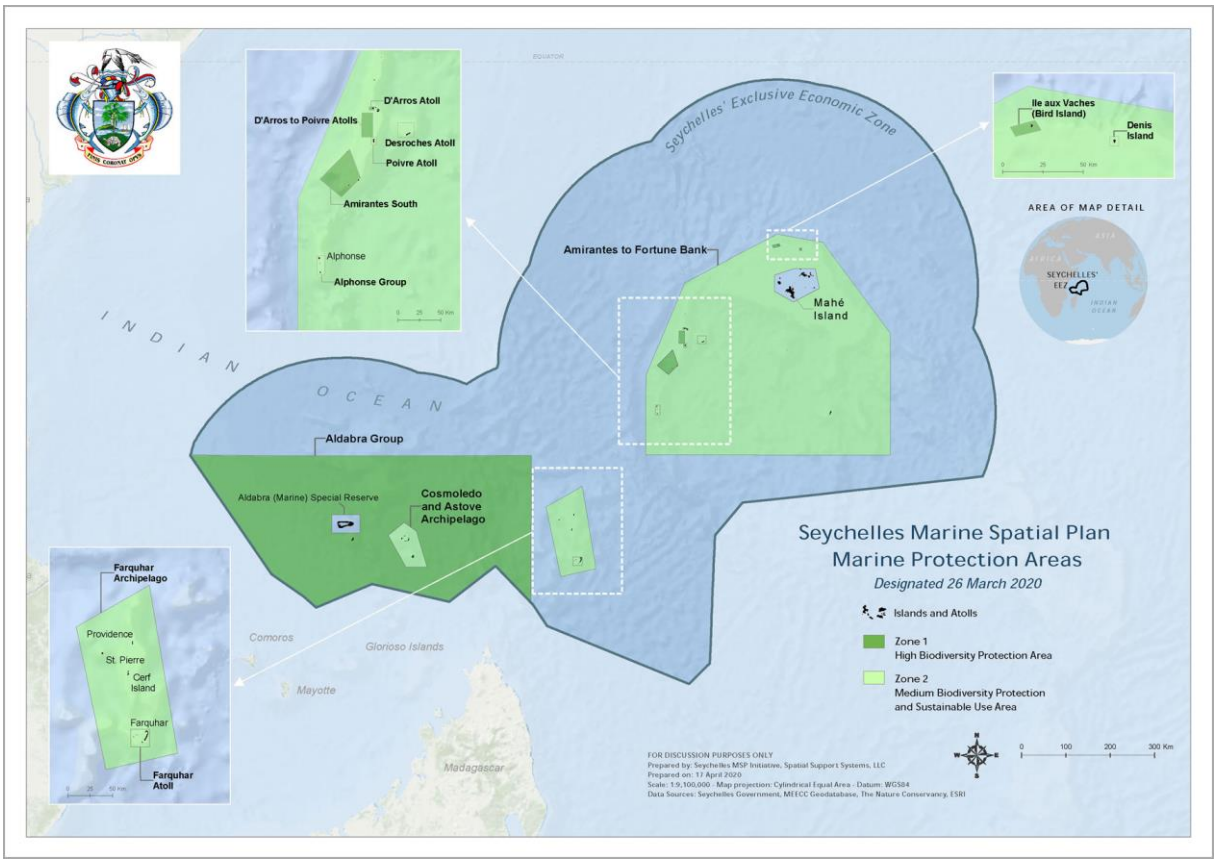

Figure 6 MPAs of high and medium biodiversity protection located in the Seychelles' EEZ (Seychelles Marine Spatial Plan Initiative 2023)

1.5 Red snapper in the Seychelles archipelago

The Emperor red snapper (Lutjanus sebae) or 'Bourzwa' in Seychellois Creole is a tropical and subtropical reef-associated fish. It has a wide geographical distribution spanning the Western Pacific and Indian Ocean (Fig. 7) (Allen 1985). Adults are typically found in depth between 10 and 100 meters in the vicinity of coral reefs (Allen 1985).

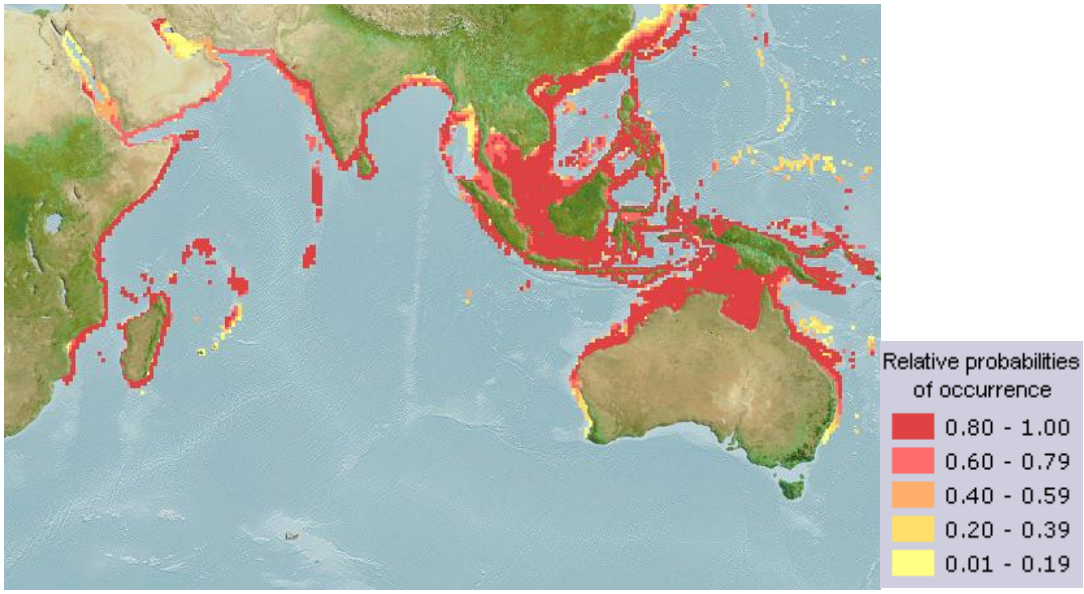

Figure 7 Probability of occurrence of the Emperor Red Snapper (AquaMaps 2019)

The Emperor snapper is caught using handlines, traps and bottom trawls. It is considered to be overexploited in the Seychelles where it is a key commercial fish along with the Brownspotted grouper (Epenephelus chlorostigma). In spite of an expansion in fishing grounds, catches have been declining since 1991 and immature fish smaller than 65cm in length represented 43% of catches in 2013 (Advance Africa Management Services 2015; GOS 2014). In particular, catches of red snappers between 2004 and 2011 were higher than the sustainable yield previously established (GOS 2014).

1.6 Objectives

As mentioned above, the high biodiversity present in the Seychelles archipelago and its reliance on fisheries as a driver of its economy make it a perfect candidate for the creation of a MPA network. The connectivity of the current network, with a focus on the Mahé Plateau, will be studied through the movement of the Emperor red snapper larvae in order to assess the connection between potential spawning grounds and existing MPAs on the inner islands. Modelling of the ocean currents is done using the 3D versions of the unstructured mesh ocean model SLIM and is followed by the creation of a particle tracker based on life characteristics of the Emperor red snapper larvae in order to simulate its movement around the area. Several questions are to be answered : how can we characterize the connectivity between reefs on the Mahé plateau and how do MPAs contribute to the dispersal of larvae? Are there any gaps in the current MPA network? which can be divided into four main objectives:

- Assessing the dynamic of larvae propagation on the Mahé plateau.
- Assessing which reefs are the biggest source of larvae for other reefs and which reefs or seagrass patches are the biggest destinations of larvae.
- Investigate if those reefs or seagrass patches are located in MPAs and if MPAs contribute to the propagation of larvae on surrounding reefs and seagrass patches.

1. Materials and methods

2.1 Area of interest

The Mahé plateau is located in the northern part of the Seychelles archipelago; in the south-western tropical Indian Ocean (Fig. 8). It spreads over a surface of approximately 40.000 km² and has a depth of around 50m on average that reaches 1000m rapidly at its limit (GOS 2014). The open ocean boundaries of the Mahé Plateau are set at the 400m isobath. As of 2020, there are eight MPAs located around the inner islands of the plateau (Fig. 9).

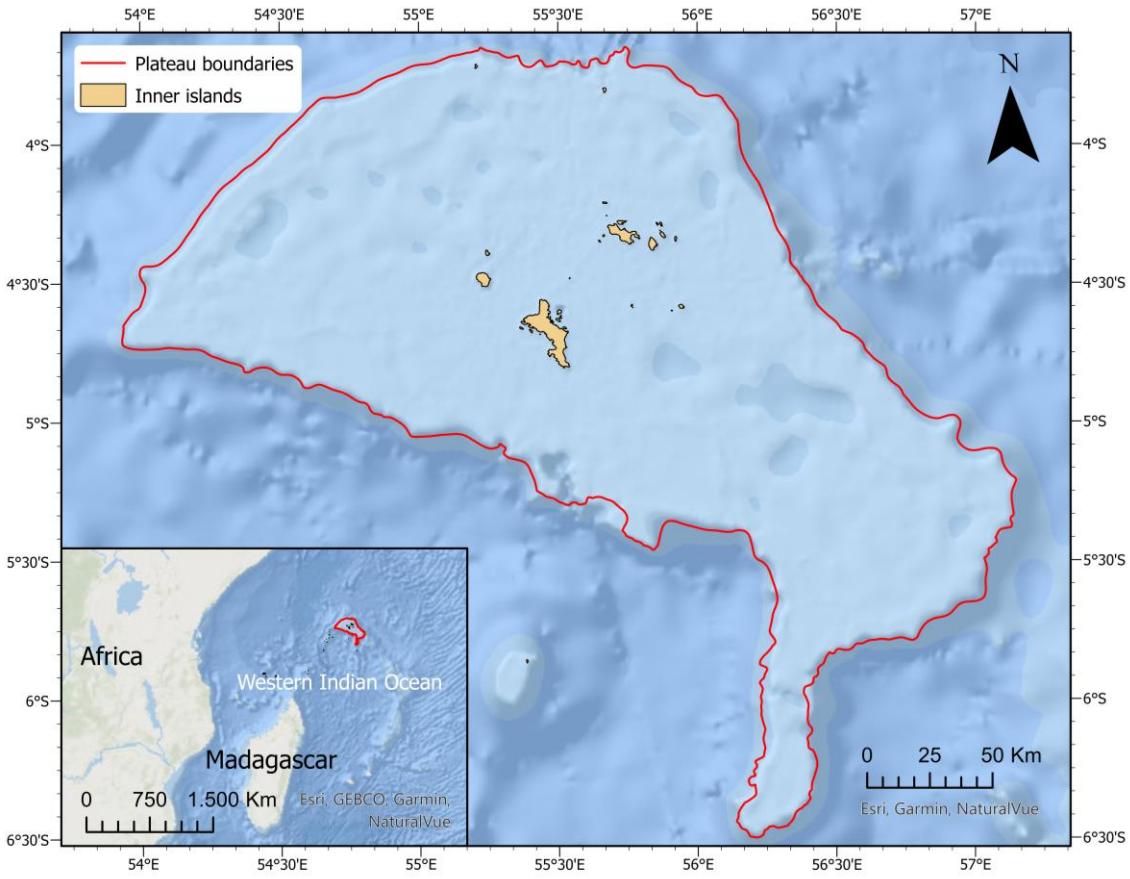

Figure 8 Mahé Plateau (Seychelles) location

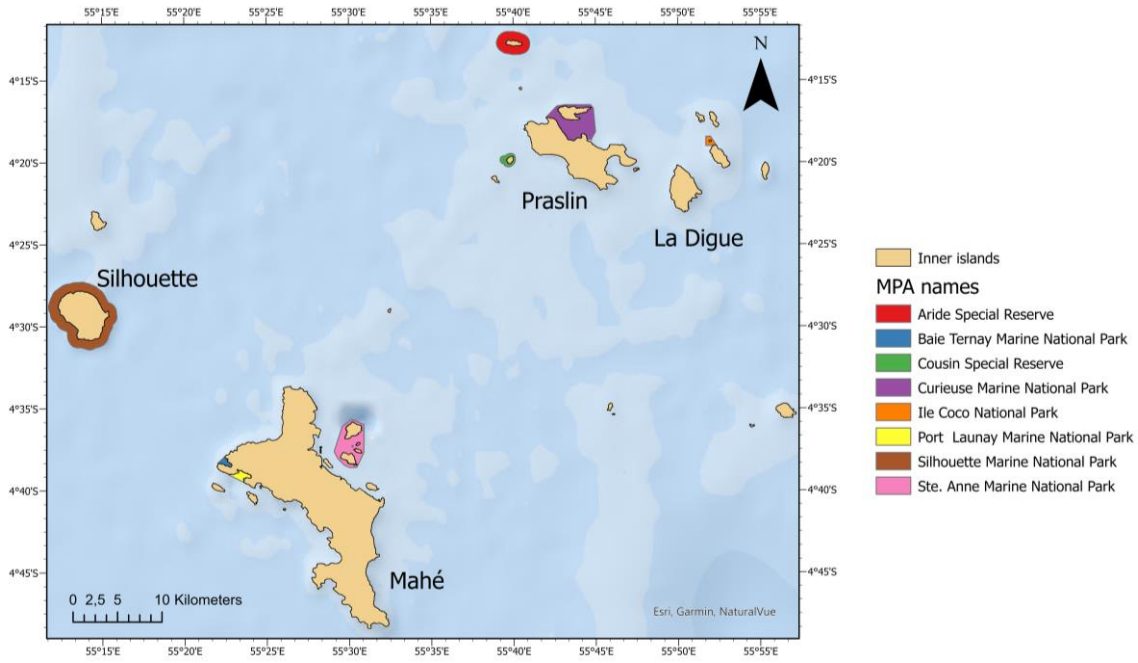

Figure 9 MPA locations and names around the inner islands

The ocean circulation on and around the plateau is driven by the seasonal monsoons coming from the south-western Indian Ocean and divided into two periods: northwesterly winds from December to March (austral summer) and southeasterly wind from April to November (austral winter). The ocean circulation is mainly wind-driven at the peak of the monsoon (from December to February and June to August) (Castillo-Trujillo et al. 2021). Water temperature near the island of Mahé reaches its warmest in April and May when it is above 29°C and its coldest in July and August when it is lower than 26°C (Castillo-Trujillo et al. 2021).

The GEBCO[1] bathymetry shows the presence of a deep area (~700m) north of the plateau (Fig. 10) which seemed unlikely because of the shallowness of the plateau. This was corrected by combining bathymetry data from nautical charts with GEBCO data through a buffer area of 2000m, allowing for a smooth transition between the two datasets (Fig. 11). Since nautical charts provide the water depth at low astronomical tide (LAT), we added half the tidal range observed during a period of a year (around 1m) to derive the bathymetry.

[1] General Bathymetric Chart of the Oceans, https://www.gebco.net/

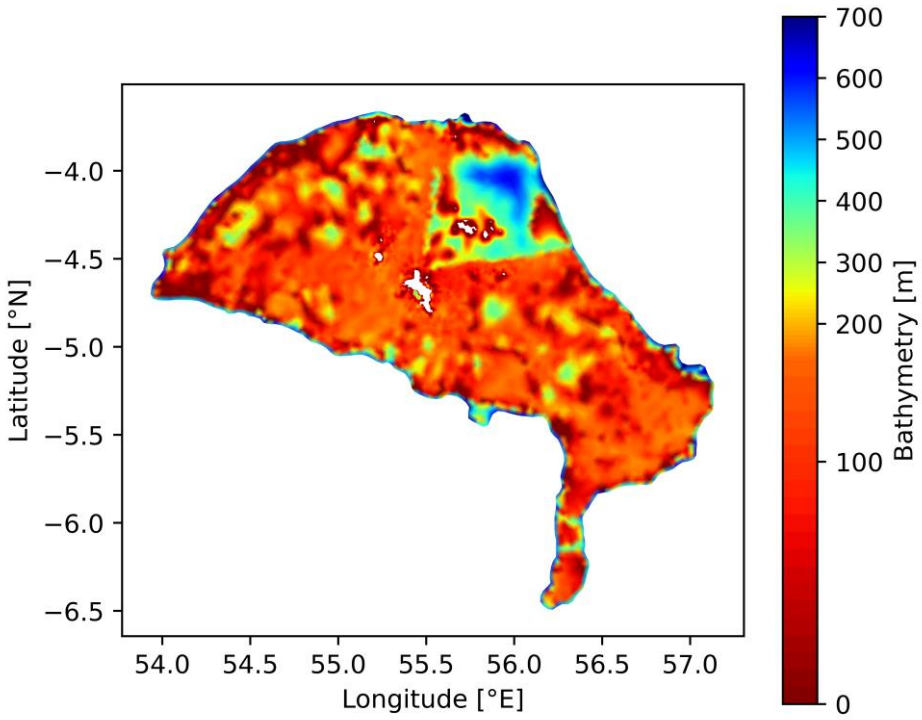

Figure 10 GEBGCO bathymetry on the Mahé plateau

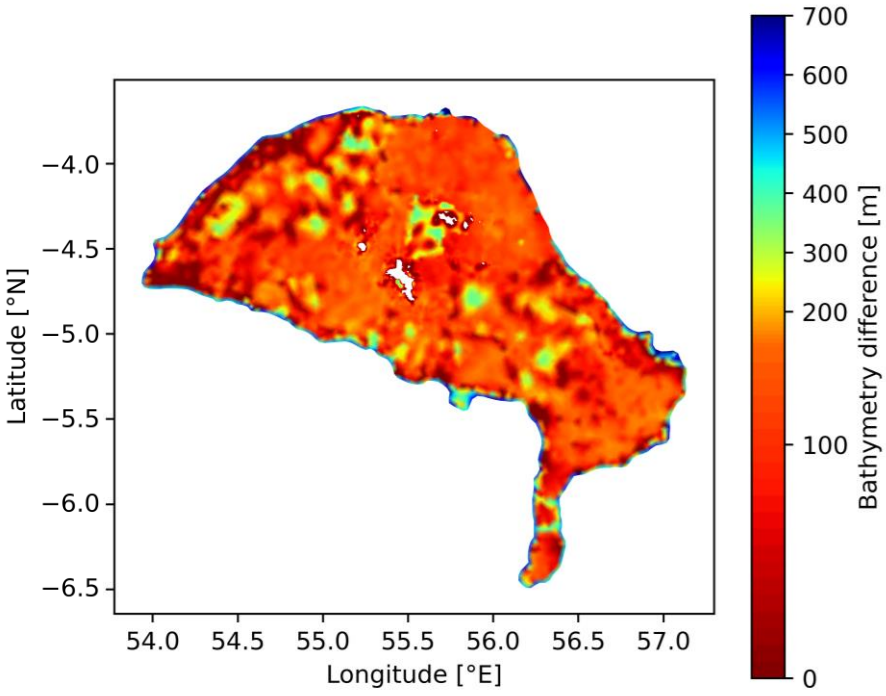

Figure 11 GEBCO bathymetry corrected using nautical maps data

2.2 General approach

This work is divided into two main parts. Firstly, the 3D hydrodynamic simulation of the area of interest. Secondly, a study of larvae dispersion and connectivity over the area of interest using a Lagrangian particle tracker built upon biological characteristics of fish larvae. Both parts are carried out using the Second-generation Louvain-la-Neuve Ice-ocean Model (SLIM)

2.3 Hydrodynamic modelling

2.3.1 SLIM model

SLIM is a hydrodynamic model that computes ocean currents by solving the equations governing the ocean circulation on an unstructured mesh. The two versions used in this work are SLIM2D and SLIM3D[2]. The 2D barotropic version of SLIM is well suited to shallower environments where the water column is well-mixed as it computes depth-averaged current velocities. It also has a smaller computational cost than 3D modelling, allowing for a finer mesh resolution.

SLIM3D uses a vertical extrusion of the 2D mesh along the depth. There exist different systems of vertical layers : the z-layers (a) remain at fixed depth, the σ-layers (b) follow the bathymetry (Fig. 12). Z-layers have constant depth levels but have the drawback of producing a staircase representation of the seabed. σ-layers, which are used in the current version of SLIM3D, follow the seabed and usually better represent the hydrodynamics when the bathymetry is not too deep . They can however be more prone to numerical issues on areas with a steep slope.

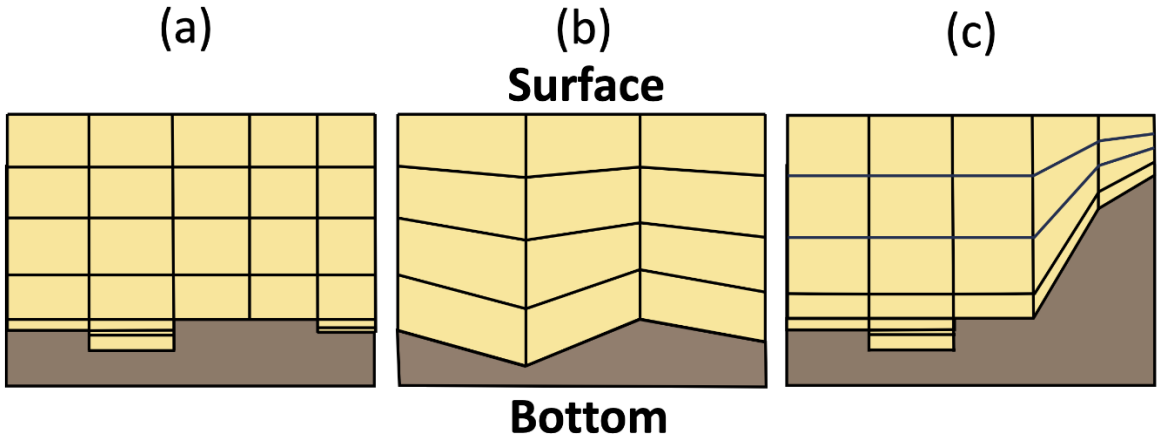

Figure 12 Illustration of the (a) z-layers, (b) σ-layers and (c) their combination

[2] **https://www.slim-ocean.be**

2.3.2 SLIM 3D : Model equations

SLIM3D solves the 3D hydrostatic equations and computes the sea surface elevation, the 3D current velocity, the salinity and the temperature on a domain Ω (Fig. 13) (Vallaeys 2018). The model equations are derived from the Navier Stokes equations under the Boussinesq and hydrostatic assumption. The Boussinesq approximation sets that density variations are neglected in all terms of the momentum equation, except the gravity term whereas the hydrostatic assumption implies that the pressure in only dependent on the height of the water column and its density.

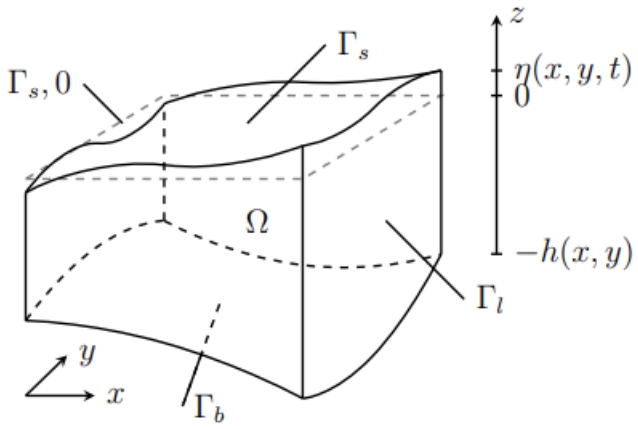

Figure 13 Sketch of the 3D domain Ω defined by its boundaries Γ. (credit: P. Delandmeter)

The domain is defined by three dimensions : x and y (the horizontal components of the position vector **x**) and z, the vertical component. The domain is limited by three boundaries : the lateral boundary Γl (open waters or shorelines), the bottom boundary Γb (the seabed) and the top moving boundary Γs(the surface of the water). h(x,y) corresponds to the bathymetry, the seafloor is thus located at z= -h(x,y) whereas the top surface is located at z= η(t, x, y). The total water depth is therefore equal to H(t,x,y) = h(x,y) + η(t, x, y).

The model equations which describe the fundamental processes driving ocean circulation are as followed :

$$\frac{\partial \mathbf{u}}{\partial t} + \nabla_h \cdot (\mathbf{uu}) + \frac{\partial w\mathbf{u}}{\partial z} = \nabla_h \cdot \left(\nu_h \left(\nabla_h \mathbf{u}\right)\right) + \frac{\partial}{\partial z}\left(\nu \frac{\partial \mathbf{u}}{\partial z}\right) - f\boldsymbol{e_z}\wedge\mathbf{u} - \frac{1}{\rho_0}\nabla_h p, \quad (1)$$

$$\nabla_h \cdot \mathbf{u} + \frac{\partial w}{\partial z} = 0, \quad (2)$$

$$\frac{1}{\rho_0}\nabla_h p = \frac{1}{\rho_0}\nabla_h pa + g\nabla_h \eta + \frac{g}{\rho_0}\nabla_h \int_z^{\eta} (\rho - \rho_0)\, dz, \quad (3)$$

$$\frac{\partial \mathrm{T}}{\partial \mathrm{t}} + \nabla_h \cdot (\mathbf{u}\mathrm{T}) + \frac{\partial(\mathrm{wT})}{\partial \mathrm{z}} = \nabla_h \cdot (\kappa_h \nabla_h \mathrm{T}) + \frac{\partial}{\partial \mathrm{z}} (\kappa \frac{\partial \mathrm{T}}{\partial \mathrm{z}}) + \mathrm{Trel},$$

(4)

$$\frac{\partial \mathrm{S}}{\partial \mathrm{t}} + \nabla_h \cdot (\mathbf{u}\mathrm{S}) + \frac{\partial(\mathrm{wS})}{\partial \mathrm{z}} = \nabla_h \cdot (\kappa_h \nabla_h \mathrm{S}) + \frac{\partial}{\partial \mathrm{z}} \left(\kappa \frac{\partial \mathrm{S}}{\partial \mathrm{z}}\right) (+\mathrm{Srel})$$

(5)

where **u** is the horizontal velocity, w is the vertical velocity, $\boldsymbol{\nabla}_h$ is the horizontal gradient operator, v_h is the horizontal viscosity, T is the temperature, v is the vertical eddy viscosity, $\boldsymbol{e}_z$ is the vertical unit vector, ρ_0 is the reference density, p is the pressure, p_a is the atmospheric pressure, η is the sea surface elevation, ρ is the density, κ_h is the horizontal eddy diffusivity, κ is the vertical eddy diffusivity, Trel and Srel are the temperature and salinity relaxation terms (Alaerts 2021; Vallaeys 2018).

The equations correspond respectively to : (1) the momentum equation, (2) the continuity equation, (3) the pressure equation, (4) the temperature equation and (5) the salinity equation. The momentum equation states that a change in momentum in a water section is due to the forces acting on it. The continuity equation states that changes in mass in a water section are equal to the difference between in and out mass fluxes. The pressure equation describes the pressure as the sum of the atmospheric pressure, sea surface elevation and baroclinic pressure.

The temperature and salinity equations are expressed through a relaxation term Srel (not computed in those simulations) and Trel which are added in order to force the computed values towards the salinity and temperature provided by a larger scale ocean model.

The relaxation of the salinity is computed as :

$$\mathrm{Srel} = \frac{\max((\mathrm{zs} + \mathrm{z}), 0)}{\mathrm{z}_s \, \tau_s} * (\mathrm{Sref} - \mathrm{S})$$

(6)

where zs is the relaxation depth, τ_s is the relaxation period, S is the salinity and Sref is the value of the variable at the ocean surface as computed from a larger scale ocean model.

The relaxation of the temperature is computed as :

$$Trel = \frac{\Delta \mathrm{z}_s \, (\mathrm{SSTref} - \mathrm{SST})}{\tau_s}$$

(7)

where $\Delta \mathrm{z}_s$ is the surface layer thickness and SST the sea surface temperature. The SST is measured through satellite data (European Union-Copernicus Marine Service 2015).

Other parameters are needed to compute the equations such as the horizontal diffusivity (κh) which is defined by the parameterization of Okubo (1971):

$$\kappa_h = c\,\Delta^{1.15}, \tag{8}$$

where c is the Okubo coefficient and Δ the mesh size. The horizontal viscosity ν_h is defined through the Smagorinsky closure scheme (Smagorinsky 1963):

$$\nu_h = \alpha\,\Delta^2 \sqrt{2\left(\frac{\partial u}{\partial z}\right)^2 + 2\left(\frac{\partial v}{\partial y}\right)^2 + \left(\frac{\partial u}{\partial y} + \frac{\partial v}{\partial x}\right)^2}, \tag{9}$$

where α is a non-dimensional constant and Δ is the square root of the surface of the horizontal section of the 3D mesh element.

The vertical eddy viscosity ν and diffusivity κ are computed from a κ-ϵ vertical closure scheme.

2.3.3 Forcing data

Ocean currents are driven by steady and time-dependent external forcings. Those forcings are the main drivers of the ocean circulation and are needed to simulate ocean currents. Time-dependent forcings include the wind, the tides and the large-scale circulation as well as the surface heat, salinity, and air temperature. Those forcings are retrieved from models and measurements in several datasets.

Winds and atmospheric pressure forcings are collected from the ERA5[3] dataset (ECMWF Reanalysis 5th generation) which provides data hourly on a 31km grid.

On its boundaries, the model is forced by a larger-scale ocean model and tides. Tidal elevation and velocity are extracted from the TPXO9 dataset (Egbert and Erofeeva 2002). Simulation outputs of SLIM were compared using two different larger-scale ocean models as open lateral boundary conditions for currents, temperature, salinity and sea-surface temperature: the The Western INDian Ocean Simulation (WINDS) and NEMO (Nucleus for European Modelling of the Ocean) (Madec et al. 2023).

WINDS is a regional ocean model with a current simulation of 1/50° (~2km) resolution (Vogt-Vincent and Johnson 2023). WINDS outputs from 1993 to 2020 are available every five days for the full 3D temperature, salinity and velocity fields, and every day for the free-surface height and depth-averaged variables. WINDS uses forcings from the ERA-5 dataset (surface air temperature, sea-surface temperature…). Its lateral boundaries are forced by a global ocean model of 1/12° resolution, GLORY12V1 and tides are extracted from the TPXO9-atlas dataset.

[3] https://www.ecmwf.int/en/forecasts/datasets/reanalysis-datasets/era5

WINDS outputs are available through the CEDA (Centre for Environmental Data Analysis) website[4]. NEMO provides daily data on a 1/12° grid (~9km) over 50 layers of depth and is available through the Copernicus Marine Service[5].

2.3.4 Mesh

SLIM relies on unstructured meshes which allow for a finer resolution closer to the coast or over regions of interest and bathymetry gradients. The mesh is computed using the seamsh python library[6]. Nodes of the triangles correspond to the points where ocean variables are computed (surface elevation, currents velocity, temperature, salinity, etc). The equations are solved numerically with the discontinuous Galerkin finite element method which does not require the solution to be continuous between neighboring elements. The mesh used during simulations is refined closer to the coast and to coral reefs (Fig. 14). It is extruded over 16 layers to form the 3D mesh.

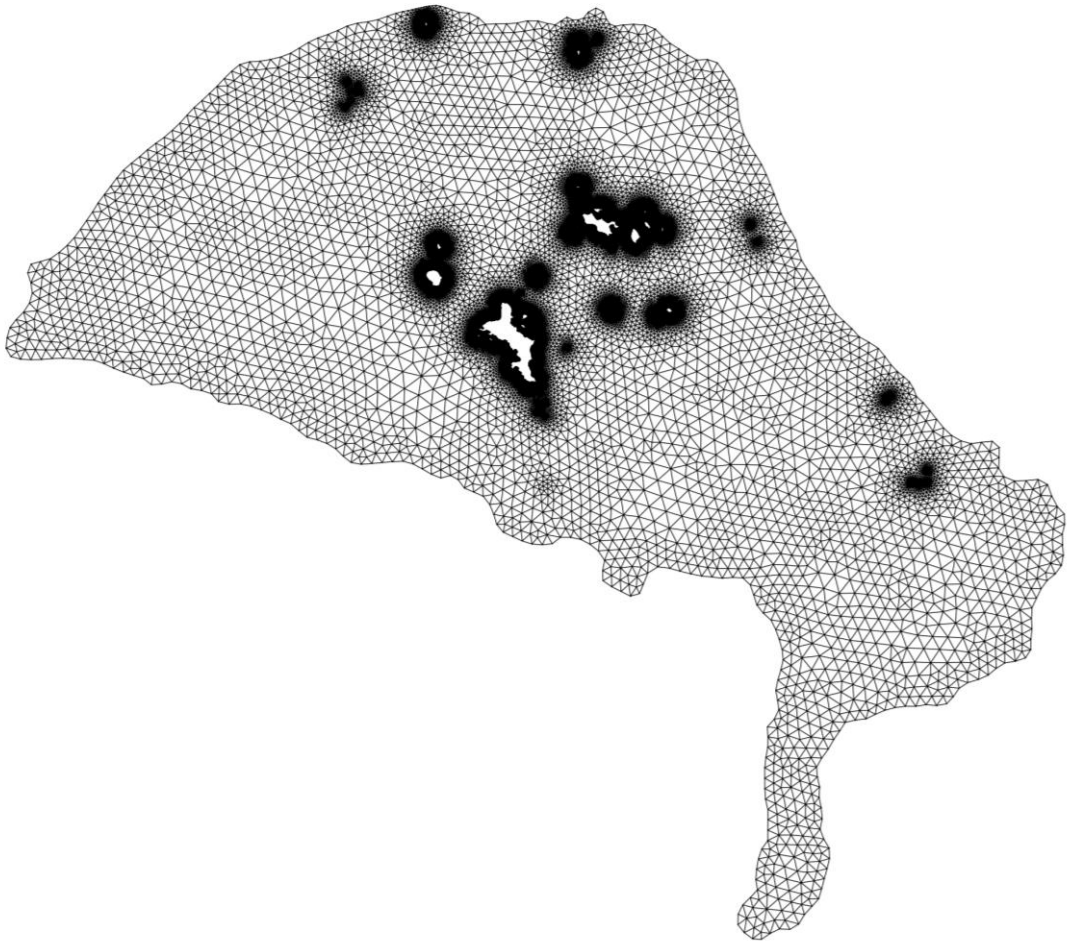

Figure 14 Mesh used for the simulations and containing 51.281 elements. The smallest element resolution is ~200m and the largest one is ~5300m

[4] https://data.ceda.ac.uk/bodc/UOX220077/
[5] https://data.marine.copernicus.eu/
[6] https://pypi.org/project/seamsh/0.3.3/

2.4 Model Validation

Validation is done through the use of tide gauges as well as ADCP (Acoustic Doppler current profiler) data collected on the Mahé Plateau which respectively record the sea level and water current velocities (Fig. 15). The sea level measurements are provided by the European Commission Joint Research Center[7]. The Seychelles Local Ocean Modelling and Observation (SLOMO) program has carried out measurements on the Mahé Plateau since 2015 which gives access to validation data through the presence of two ADCPs (Scripps Institution of Oceanography et al. 2017) for the year 2017 (northern ADCP) and 2018 (eastern ADCP).

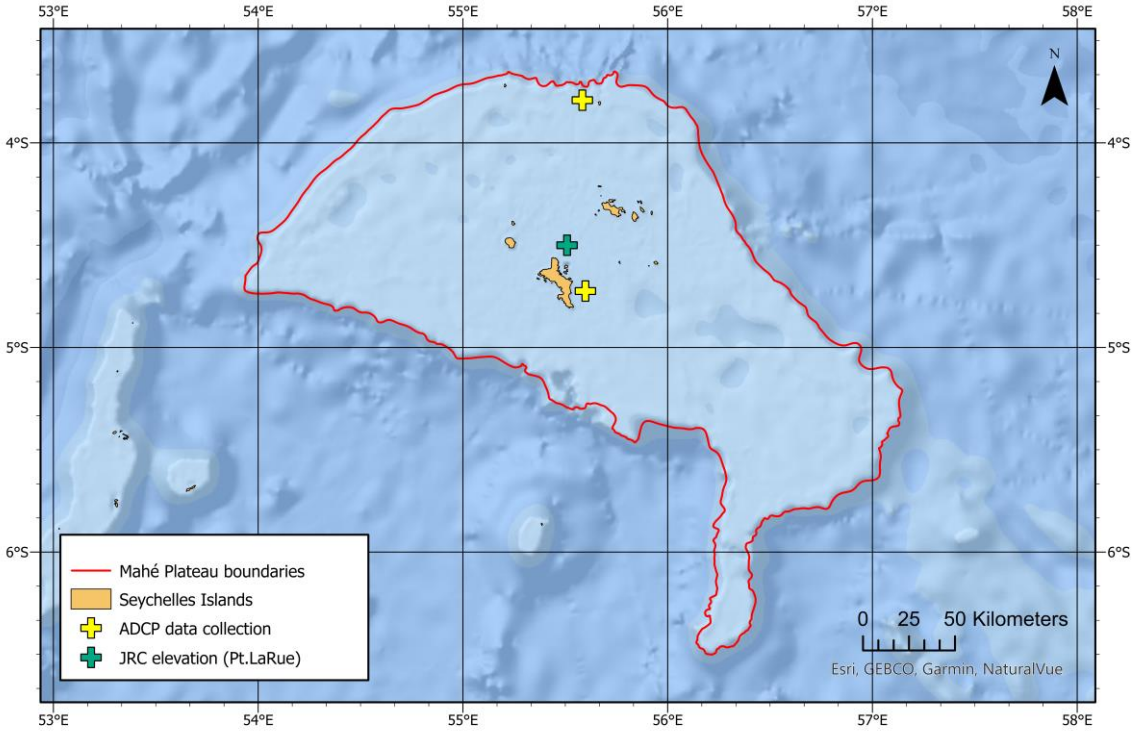

Figure 15 Location of the ADCP installed for the SLOMO project on the plateau as well as the JRC tide gauge (Seychelles-Pt. LaRue)

Because of the long computation time of 3D simulations and the size of the outputs, the period used for all the comparison between simulations using WINDS and NEMO takes place over two month and a half, between January 1 and the March 15, 2018. The data recorded during this period at the eastern ADCP (ADCP-E) is used for the validation.

[7] https://webcritech.jrc.ec.europa.eu/SeaLevelsDb/Device/925

2.5 Circulation of fish larvae

2.5.1 Lagrangian Particle tracker

The step following the hydrodynamic modelling of the area is the simulation of the dispersion of fish larvae. This process is achieved by using a Lagrangian Particle tracker integrated within SLIM3D. A Lagrangian tracker coupled with SLIM 2D and 3D has been repeatedly used before to model the dispersal of drifting material, including coral larvae (Frys et al. 2020) or stone crab larvae (Alaerts et al. 2022). This method allows for each particle to have its own characteristics and behaviors.

The 3D position of each particle is computed with the following advection-diffusion equation:

$$d\mathbf{X}(t) = (u + \nabla \cdot \mathbf{K})\, dt + \sqrt{2\mathbf{K}dt}\ \cdot \mathbf{R}(t), \tag{10}$$

where **X**(t) is the time-dependent 3D position vector, u the particle velocity (buoyancy and current velocity), **R**(t) is a vector of random numbers with zero mean and unit variance and **K** is the turbulent diffusivity tensor:

$$\mathbf{K} = \begin{bmatrix} \kappa_h & 0 & 0 \\ 0 & \kappa_h & 0 \\ 0 & 0 & \kappa \end{bmatrix}, \tag{11}$$

The first part of the equation $(u + \nabla \cdot \mathbf{K})$ is related to advection and combines the particle velocity obtained by summing its own buoyancy with current velocity with $\nabla \cdot \mathbf{K}$ which includes a correction drift to prevent accumulations of particles in regions of low diffusivity (Gräwe and Wolff 2010; Scherpereel Colin 2022). The second part, $\sqrt{2\mathbf{K}dt}$, is related to random diffusion.

Exchanges between sub-areas of the plateau are studied trough the computation of connectivity matrices of which rows and columns correspond to sources and sinks (reefs and seagrass patches) of particles (larvae in this case). An entry (i, j) in the connectivity matrix corresponds to the number of larvae released from the area i to the area j. In this case, the connectivity matrix is built by adding a value of 1 to the relationship between two reefs every time a larvae settles.

2.5.2 Indicators

Graph-theory indicators can serve as tools to understand and highlight the connectivity differences between areas. Graph theory has been used to study landscape connectivity (Galpern, Manseau, and Fall 2011; Urban and Keitt 2001) as well as population connectivity in marine conservation (Anadón et al. 2013; Treml et al. 2008) and to implement the concept of connectivity in MPAn evaluation (Assis et al. 2021; Friesen et al. 2019).

Firstly, the **In-degree** (ID) and the **Out-degree** (OD) are computed on a non-normalized matrix and respectively correspond to the incoming and outcoming edges of the considered reef which would, in this case, correspond to the potential of a reef to receive fish larvae or to send fish larvae to other reefs.

Secondly, the **weighted connectivity length** (WCL) computes the average distance travelled by larvae from a given area. It is calculated through the following equation:

$$WCLi = \frac{\sum j(\widetilde{C_{ij}} * dij)}{\sum j\widetilde{C_{ij}}},$$

(12)

Where dij is the distance between habitats i and j and $\widetilde{C_{ij}}$ is the normalized element of the connectivity matrix (Alaerts et al. 2022; Dobbelaere et al. 2020).

Thirdly, the **self-recruitment** (SR) serves as way to measure the isolation of an area in the network. It corresponds to the fraction of larvae that were produced in the area and did not leave it. It corresponds to the following equation :

$$SRi = \frac{C_{ii}}{\sum jC_{ji}},$$

(13)

where Cii is the element of the connectivity matrix.

Finally, the **local retention** (LR) is the fraction of larvae spawned by a reef that settled on that same reef.

$$LRi = \frac{Cii}{Si},$$

(14)

where Cii is the element of the connectivity matrix and Si the number of seeded larvae.

2.5.3 Larvae behavior

Life stages and characteristics of the larvae were based on the work of Zhou et al. (2024) which modelled the larval dispersal of the Red Snapper (Lutjanus campechanus) in the Northern Gulf of Mexico. The pelagic larvae duration (PLD) is divided into five stages with specific characteristics (Fig. 16): (1) Egg, (2) Pre-flexion stage, (3) Flexion, (4) Post-flexion, (5) Settlement.

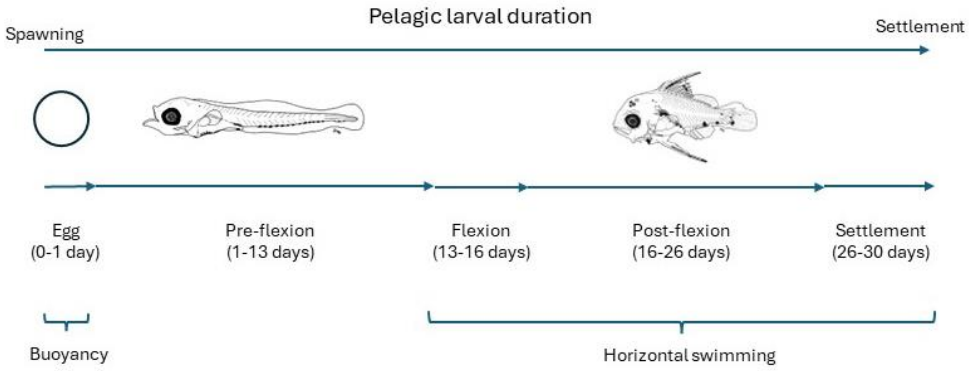

Figure 16 Pelagic larval stages and duration of Lutjanus campechanus, based on (Leis 2020, 20; Zhou et al. 2024), images from (Drass et al. 2000)

The presence of a positively buoyant egg stage has shown to lead to more field-accurate results while modelling the dispersal of fish larvae as it allows eggs to reach the surface water and move downwind (Leis 2020). The positive buoyancy is a result of the water density and the anatomy of the egg which impacts its density. The buoyancy of the Red snapper egg is calculated using the following Stokes equation (Paris et al. 2013):

$$Wb = g \times d \times d \times \frac{\rho water - \rho egg}{18\mu}, \quad (15)$$

where Wb is the buoyancy vertical velocity (m/s), g is the gravitational acceleration (m/s^2), d is the egg diameter (m), ρwater and ρegg are the density of the water and egg (kg/m^3) and μ is the water molecular viscosity (kg/m*s) computed as follows:

$$\mu = 1{,}88 \cdot 10^{-3} - (T * 4 \cdot 10^{-5}) \quad (16)$$

where T is the temperature of the water (°C), here fixed at 27°C

Bourque and Phelps (2007) measured a d value of 0.08cm for the Lutjanus campechanus. Sundby and Kristiansen (2015) set that pelagic eggs have an density comprised between 0.001 and 0.006 g/cm3 with most of them being between 0.001 and 0.002g/m3 less than medium seawater. The value used here is 0.0015 g/m^3.

Emperor red snapper spawning on the Mahé plateau happens all year round with peaks in March and September (Advance Africa Management Services 2015). Simulations are thus done over the first six months of 2018, from January to June and in September. Spawning happens every 24 hours at the depth of the coral reefs during the first ten days of each month except in January when it happens as one batch on the tenth to account for the spin up period of the simulation. Larvae are spawned at a density of 50 larvae per km^2 everyday which totals to around 10^5 larvae each month.

Aggregations and spawning of snappers are known to happen on the Mahé plateau but little information is known about their exact location apart from the fact that they take place around the inner islands and on certain offshore areas (Grandcourt et al. 2008). The hypothesis is thus made that spawning happens from reefs located on the plateau as Emperor red snappers are known to be present in their vicinity (Allen 1985). Coral reefs are extracted from the UNEP global distribution of coral reefs data set (UNEP-WCMC et al. 2010).

Fish larvae develop horizontal swimming abilities during the notochord flexion stage. The speed of fish larvae increases during the flexion speed to reach its maximum set at 41 cm/s (Fisher et al. 2005; Zhou et al. 2024). This allows fish larvae to swim towards seagrass meadows and reefs which are within a detection distance of less than five kilometers.

Larvae can settle when they are above reefs or seagrass patches with a settling velocity of 0.0002 m/s. They are considered 'settled' once they reach a depth of 1m above the reefs. After the duration of the pelagic state, 30 days, larvae are removed from the simulation.

2.5.4 Coral and seagrass location

Spawning takes place from coral reefs located on the plateau. Two sources were considered for the location of the coral reefs, the Allen Coral Atlas (ACA) (Lyons, Larsen, and Skone 2022) and The Global Distribution of Coral Reefs established by the UNEP World Conservation Monitoring Centre (UNEP-WCMC) and the WorldFish Centre (UNEP-WCMC et al. 2010). Both datasets show similar coral reefs repartitions with the ACA dataset displaying a larger number of smaller offshore reefs (Fig. 17). The number of entities present on both datasets varies : the UNEP-WCMC dataset counts 115 polygons whereas the ACA counts 13309, many of them being smaller sized (4437 being smaller than 25 square meters) (Fig. 18).

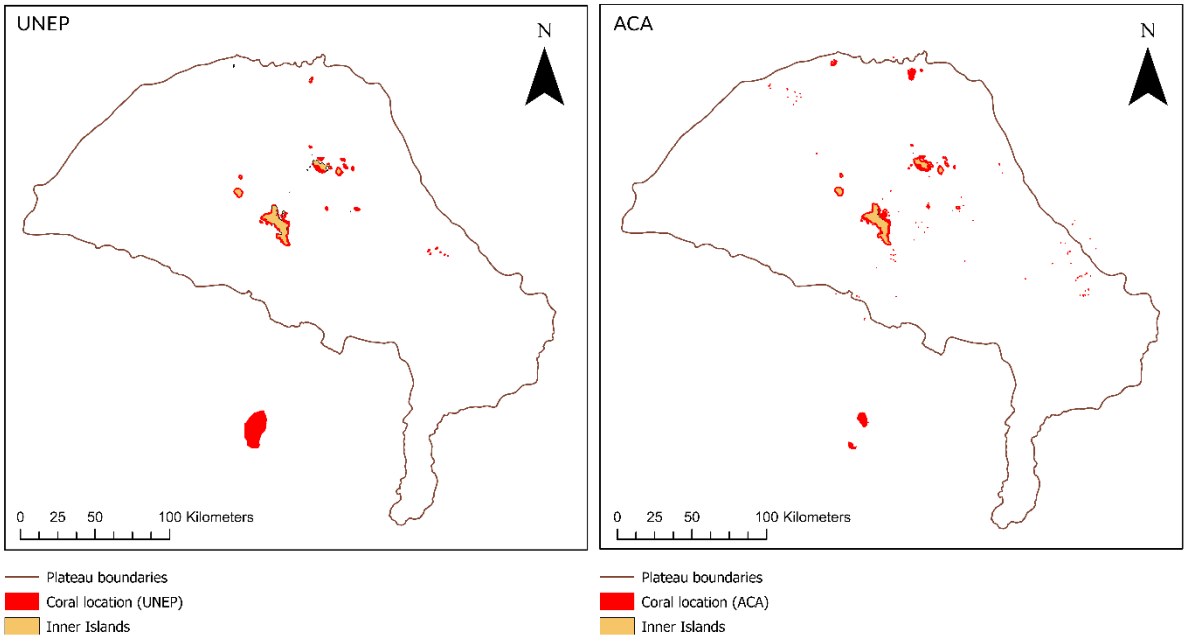

Figure 17 Comparison of coral location between the UNEP and ACA datasets on and around the Mahé plateau

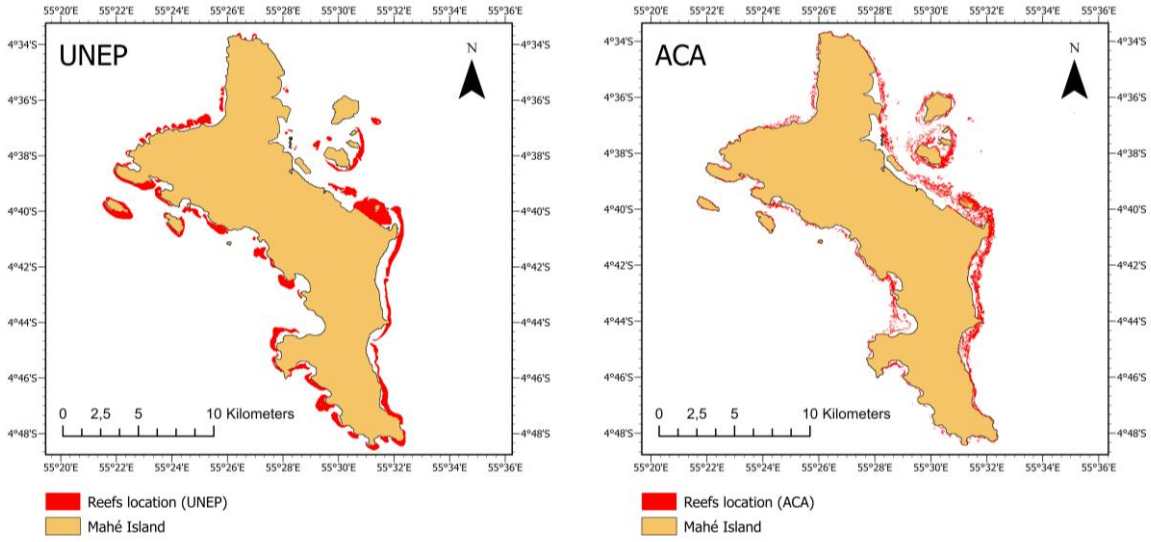

Figure 18 Comparison of coral location between the UNEP and ACA datasets around Mahé island

The UNEP dataset was finally used as spawning grounds and reef polygons were used to create squared entities of 500m x 500m (the size of the smallest reefs) in order to have consistent-sized reef, leading to a final number of 779 polygons considered.

Larvae are able to settle on reefs and on seagrass meadows which are located around the inner islands (Fig. 19). The number of larvae settling on reefs and on MPAs is recorded during the entire simulation. MPA locations established by the Seychelles Marine Spatial Plan[8] were provided by the Amanda Port-Louis (Ministry of Agriculture, Climate Change & Environment) and seagrass location data by Dr. Jérôme Harlay (University of Seychelles).

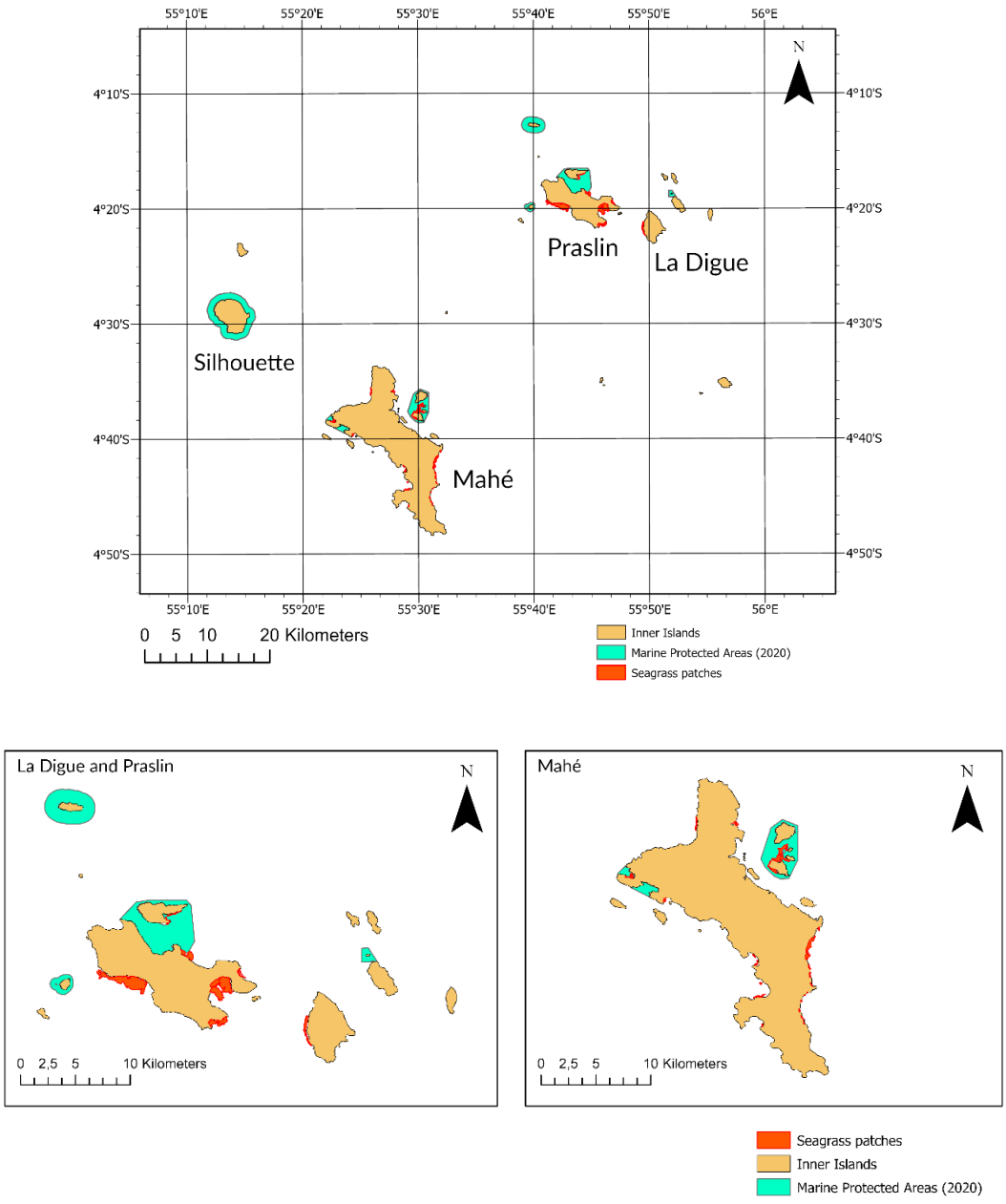

Figure 19 Seagrass and MPA location around the inner islands

[8] https://seymsp.com/

3. Results

In this section we present the results obtained. First we compare the output of SLIM3D using two different large-scale oceanic currents forcing (i.e. WINDS and NEMO). Then we present the output of the hydrodynamic model obtained over seven month, from January to June and in September 2018. Finally, we present the results of the connectivity analysis performed on the reefs and MPAs of the Mahé plateau.

3.1 Model validation

3.1.1 NEMO and WINDS comparison

Before the final hydrodynamic simulation of seven months, we first validated the simulated velocity field with respect to ocean currents velocity measurements at ADCP-E (see location in Fig. 15) from January 1 to March 15, 2018. As we have two different large-scale oceanic currents forcing (i.e. NEMO and WINDS), we ran simulations with SLIM3D forced by each of these models on the open boundaries.

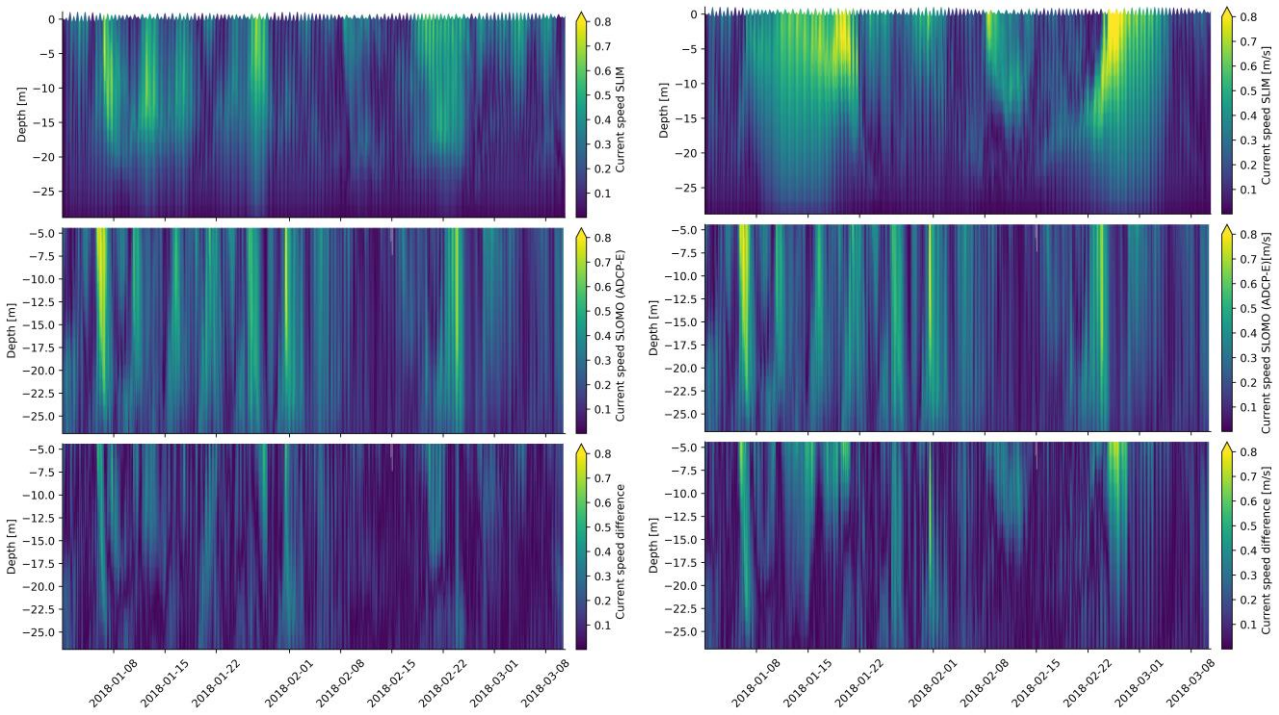

Figure 20 Simulated (top row) and observed (middle row) current speed (m/s) profiles between Jan. 1 and March 15, 2018 when forcing SLIM with CMEMS/NEMO (left) and WINDS (right) on the open boundaries. The last row shows the difference between the observed and simulated current speed.

The simulated current speed is closer to the observed current speed when using NEMO than when using WINDS on the open boundaries (Fig. 20). NEMO seems to better represent the variations in current speed with a period of a few days observed during the first half of the simulated period. However, in both cases the current speed is lower below 20m than it is in the observations. Similar results are observed in the current direction (Fig. 21).

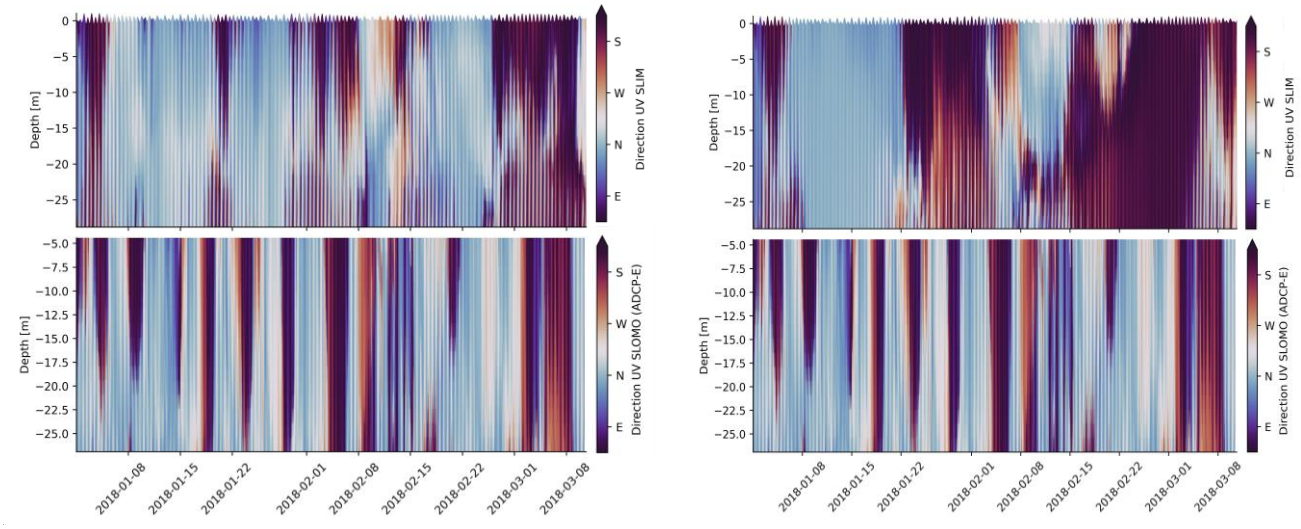

Figure 21 Simulated (top row) and observed (middle row) current direction profiles between Jan. 1 and March 15, 2018 when forcing SLIM with CMEMS/NEMO (left) and WINDS (right) on the open boundaries.

Both simulations lead to the following root-mean-square error (RMSE) values:

Component	SLIM forced with NEMO	SLIM forced with WINDS
u (m/s)	0.134	0.159
v (m/s)	0.209	0.330
uv (m/s)	0.152	0.185
uv dir (°)	16.961	22.485

Table 1 RMSE values of outputs calculated between the 01/01/2018 and the 15/03/2018

The simulated velocity field at a five-meter depth, obtained when forcing SLIM with NEMO represents most but not all variations in speed direction recorded at the ADCP-E, notably around mid-January (Fig. 22).

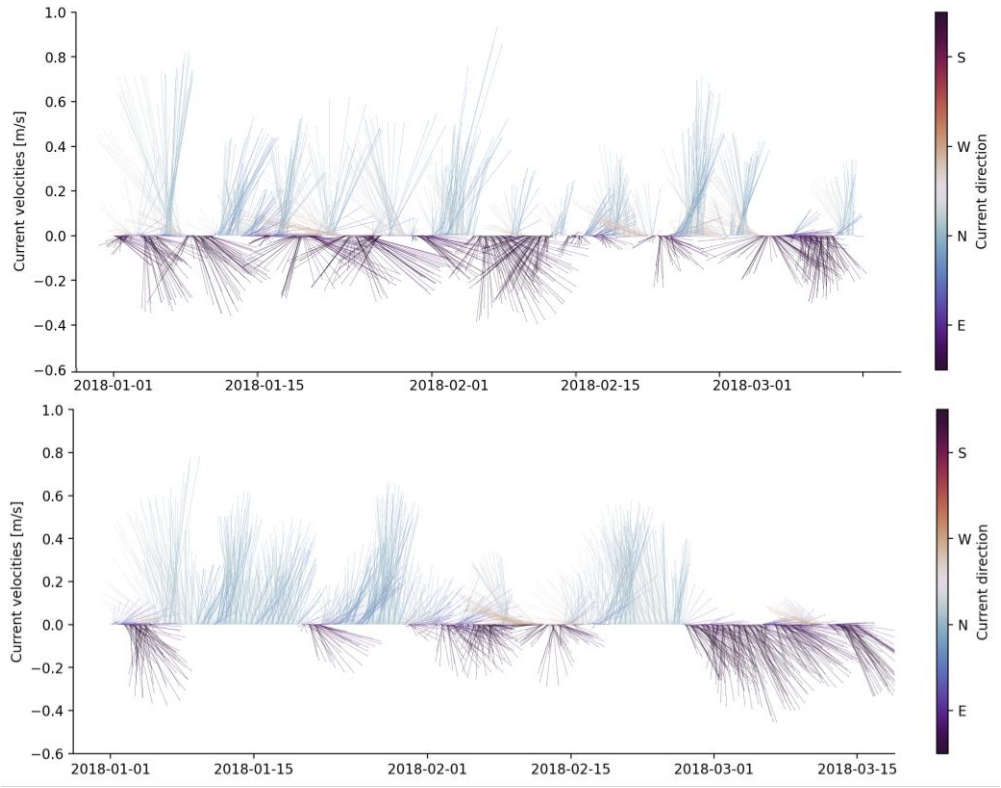

Figure 22 Current velocity (m/s) and direction recorded by the ADCP-E (top) and output by SLIM (bottom) at the ADCP location for a depth of 5 meters between 01/01/20108 and 15/03/2018 using NEMO as larger scale ocean model

To explain this difference, winds from the ERA-5 model were compared to wind velocity measurements at the Seychelles Airport located on Mahé. It appears that the measured wind velocity was almost twice as high as the velocity predicted by the ERA-5 during the month of January (Fig. 23). We tried to double the amplitude of the ERA5 wind forcing used in the SLIM simulations but it did not lead to significant changes in the simulation. It however suggests that using a regional atmospheric model with a spatial resolution finer than the global ERA5 dataset might improve the model results.

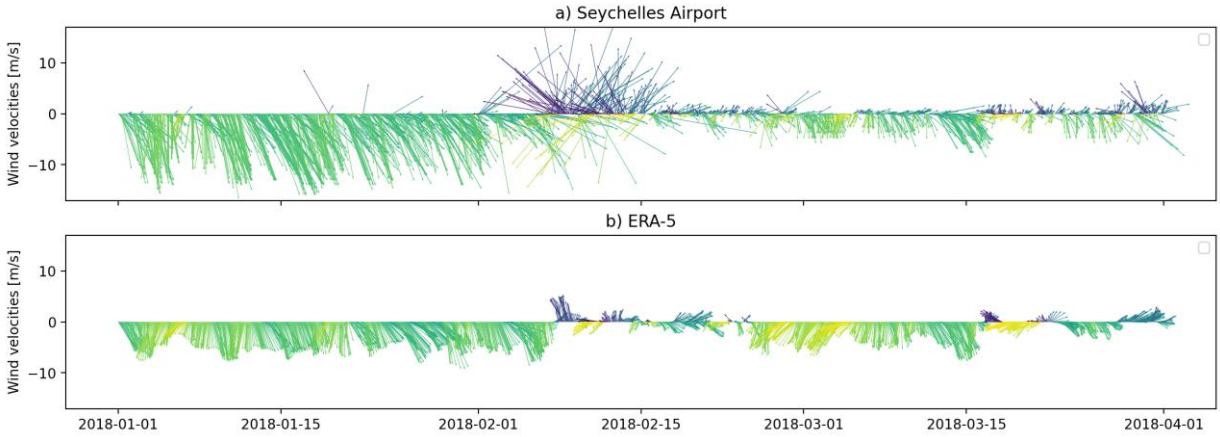

Figure 23 Wind field measured at the Seychelles Airport (top) compared with the ERA5 wind (bottom) at the same location.

3.1.3 Hydrodynamic simulation

The final hydrodynamic simulations take place over two periods of time: from January 1 to June 31 and from August 20 to October 10, 2018, leaving a spin up period of 10 days before the spawning of larvae in September. The first 10 days of January are not comprised in the following results to account for this spin up period.

As stated previously, the ocean circulation over the Mahé plateau is influenced by two monsoon seasons. The northwest monsoon season happens during the austral summer (between December and March) when winds are southeasterly and the southeast monsoon during the austral winter (between April and November) during which winds are northwesterly. The SLIM3D model simulates northeasterly currents from January to March which shift northwesterly during the month of April (Fig. 24).

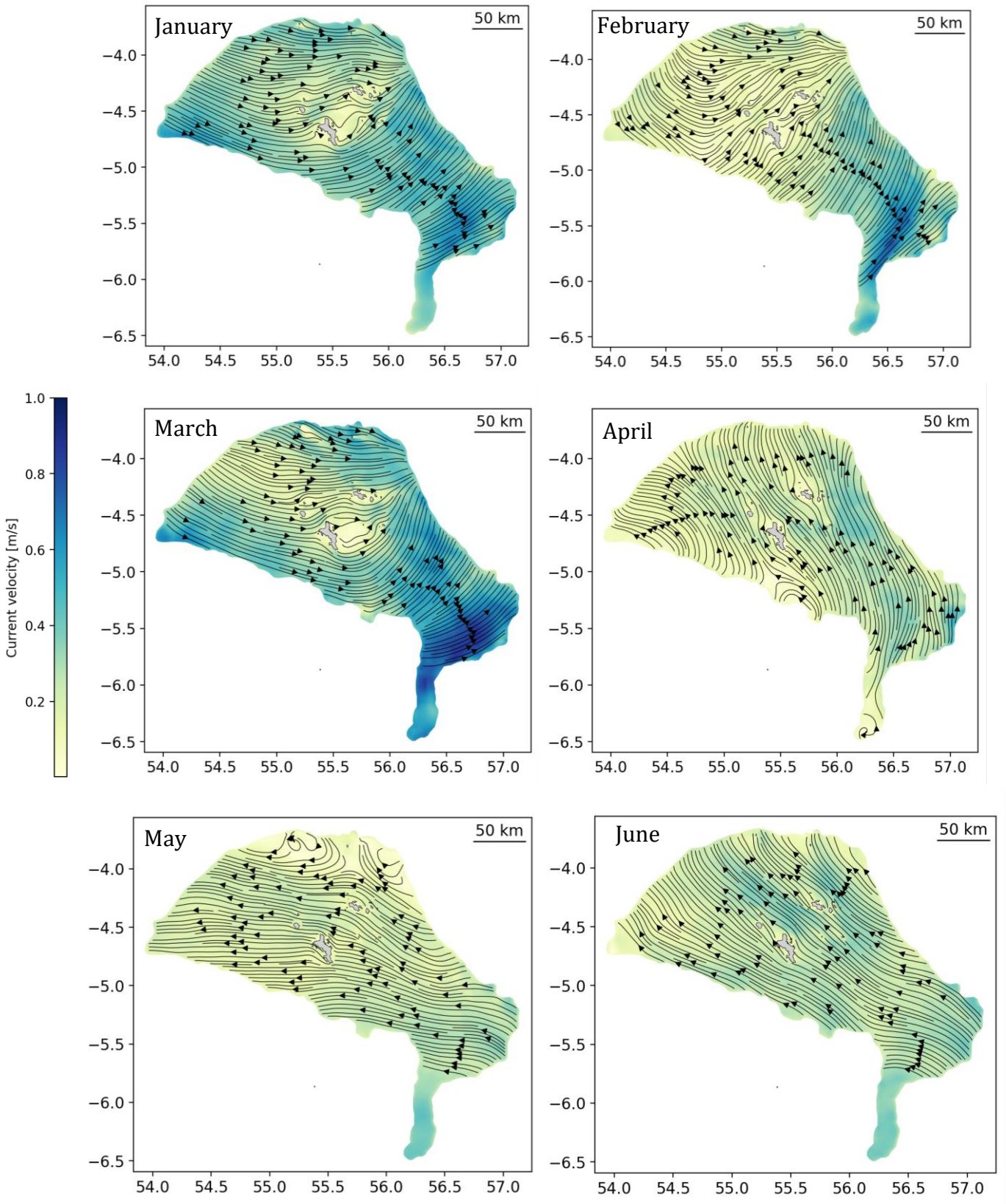

Figure 24 Monthly averaged surface current speed and direction from January to June 2018

The month of September was also simulated in order to have an idea of the currents direction and velocity later in the year during another month of peak spawning. Currents simulated with SLIM3D mostly flow north-westward (Fig. 25).

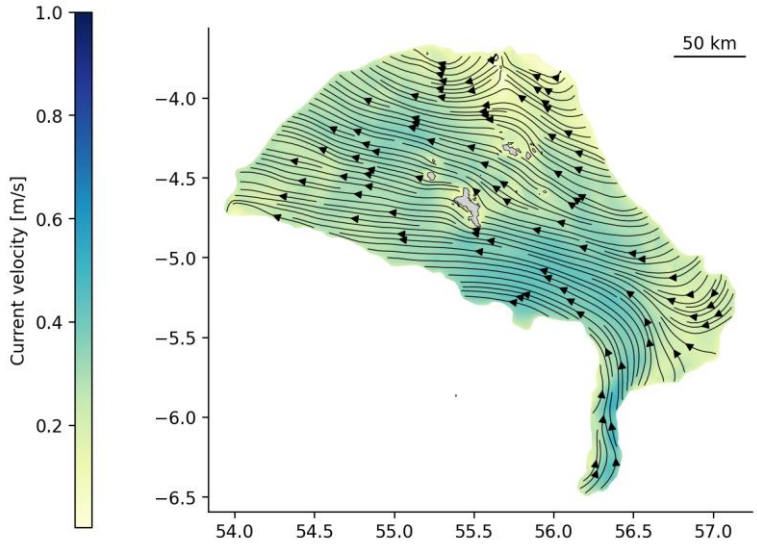

Figure 25 Averaged surface current speed during the month of September 2018

As stated previously, water temperatures around Mahé island are known to reach more than 29°C in April and May and less than 26°C in July and August. The output of SLIM3D at the ADCP-E location (see location in Fig. 15) shows temperatures in qualitative agreement with that trend. The simulated temperature can reach 31°C near the surface in February and are above 28°C through the entire water column in March. Those temperatures stay above 29°C from April to the middle of May when they begin lowering to reach 25°C at the end of June (Fig. 26). The water temperatures and salinity (Fig. 27) are mostly constant over the depth and show limited vertical stratification, although there is some in February when surface waters warm up the most.

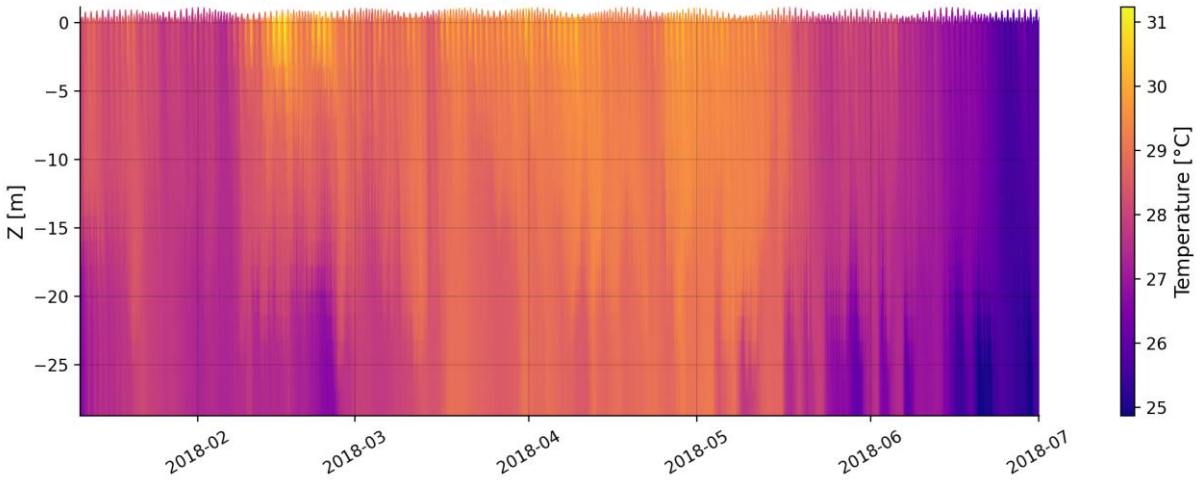

Figure 26 Temperature profile obtained with SLIM3D at the ADCP-E location

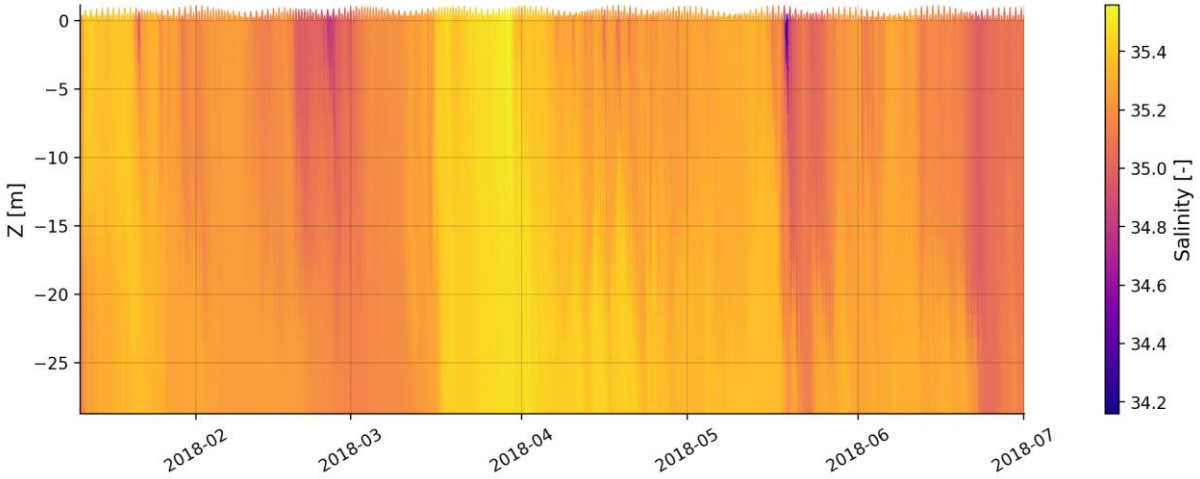

Figure 27 Salinity profile obtained with SLIM3D at the ADCP-E location

South-east of the ADCP-E, 80km away from Mahé , where the depth is higher (~85m), the vertical temperature and salinity profiles are more stratified (Fig. 28, 29). There is especially a difference above and below 50m where the temperatures drop from around 25°C to around 20°C. Temperatures rise at the beginning of March and lower at the beginning of May but stay above 26°C at the surface during the entire simulation. In both locations, salinity rises during the second half of March.

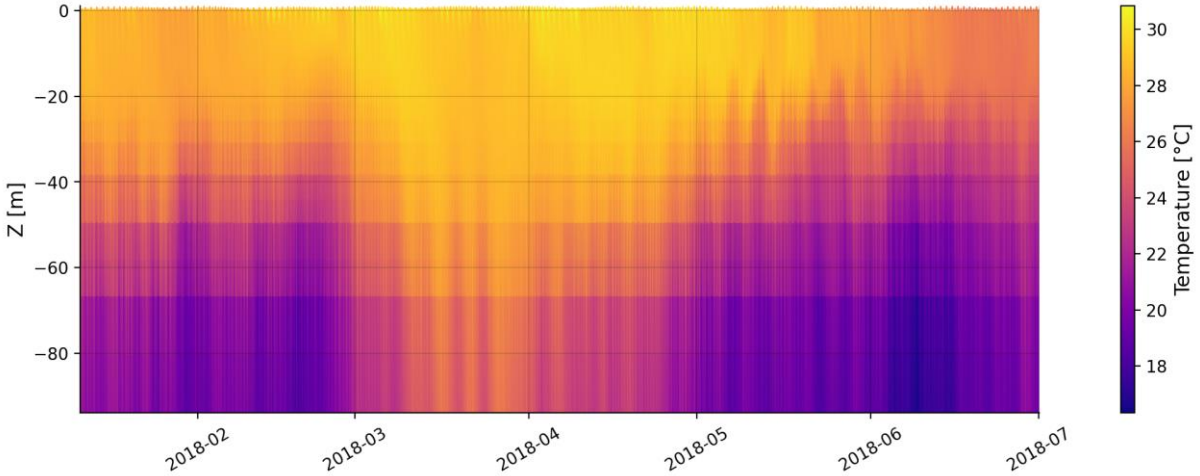

Figure 28 Temperature obtained with SLIM3D profile at coordinates [56.00, -5.3]

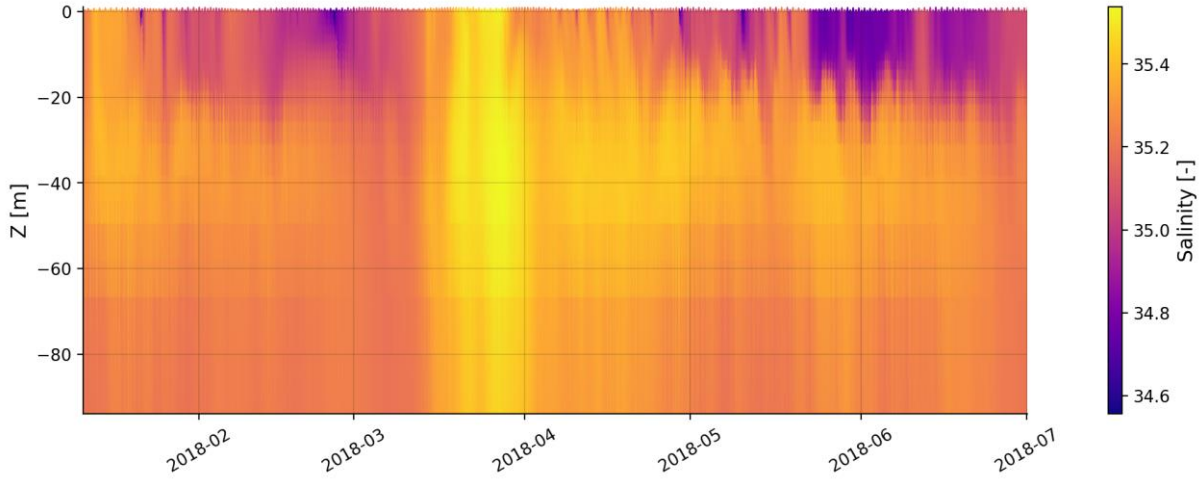

Figure 29 Salinity profile obtained with SLIM3D at coordinates [56.00, -5.3]

The sea-surface elevation during the six months can be compared to the sea-surface elevation recorded at the JRC Pt. LaRue tide gauge (see location in Fig 15.) The RMSE computed over the six months is 0.057m. The simulated values replicate the observed values well, however, the observed value have a slightly larger amplitude than what is obtained through the simulation (Fig. 30).

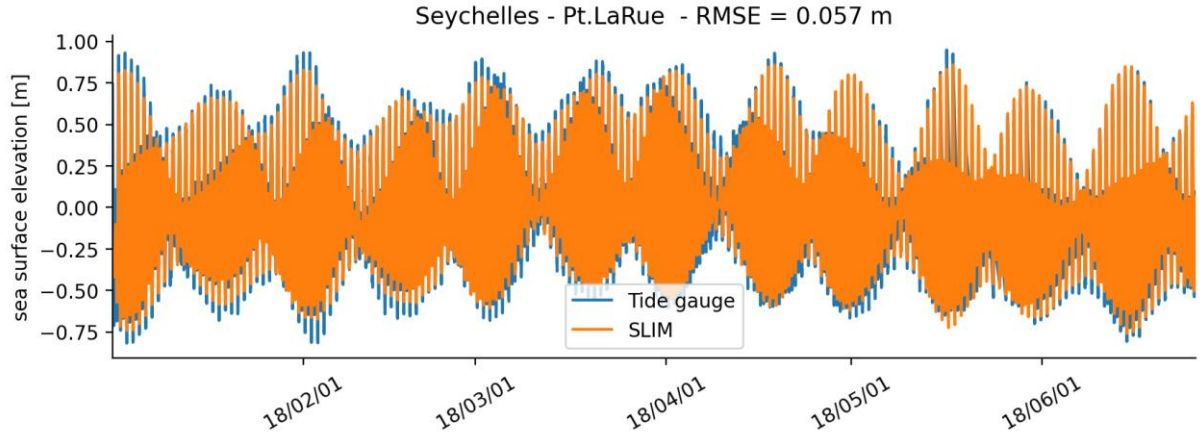

Figure 30 Sea surface elevation modelled by SLIM and measured at the JRC Pt. LaRue tide gauge

3.2 Larvae dispersal

This section presents the results obtained with the LPT model using hydrodynamic simulations spanning from January to June and September 2018. As stated previously, larvae are spawned during the first ten days of each month at a density of 50 larvae per km^2 , which amounts to a total of $\sim 10^5$ larvae released per month. We assessed the sensitivity of our results to the presence and absence of a positive buoyancy during the 'egg' stage. The connectivity between MPAs and between reefs on the MP was then investigated through the use of connectivity indicators.

3.2.1 General settlement

Larvae are spawned on reefs during the first ten days of each month and leave the plateau at a high rate (Fig. 31), especially during month where the current velocity is higher, namely January and March (Fig. 24). In January and March as well as in June and September, when currents have shifted northwesterly, most larvae have left the MP about 10 days after their spawning hence before developing active swimming. The lowest percentages of larvae leaving the MP are observed in February and May.

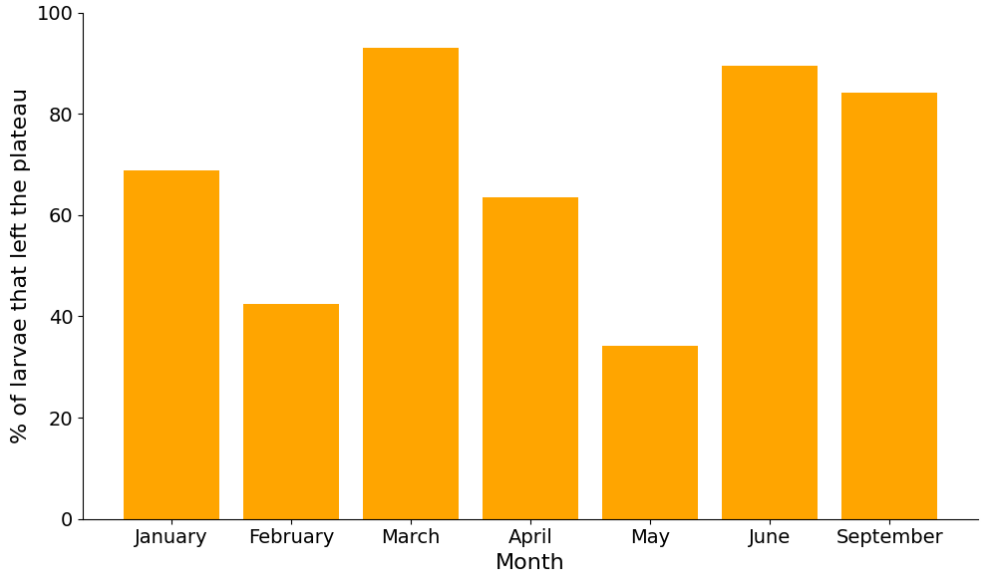

Figure 31 Percentage of larvae spawned during each month and leaving the Mahé plateau.

Larvae can settle on reefs and seagrass patches. The lowest settling percentage (i.e. the percentage of spawned larvae that settled on reefs during a particular month) happens in June when it reaches only 0.5% while the highest settling rate occurs in January, reaching 12.5% (Fig. 32).

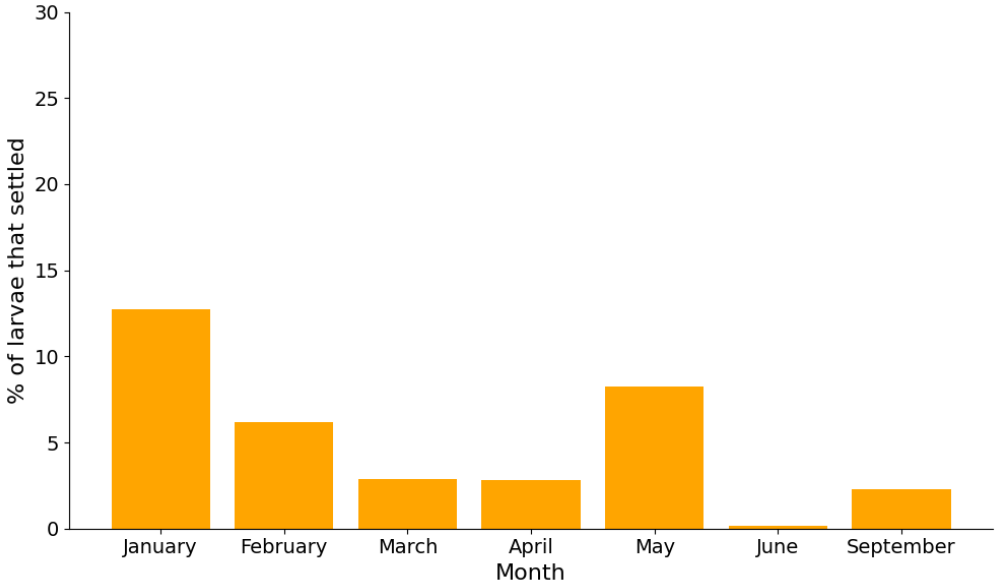

Figure 32 Percentage of larvae settling on a reef during their PLD

3.2.2 Impact of buoyancy

In order to quantify the impact of the positive buoyancy on the propagation of larvae, the same simulations were carried out without buoyancy during the first 27 hours. The difference in larvae leaving the MP is lower without buoyancy during all months but March (Fig. 33). This difference lies between 2 and 10%. The impact of buoyancy on leaving larvae is however variable with less larvae settling for all months but February, April and June (Fig. 34).

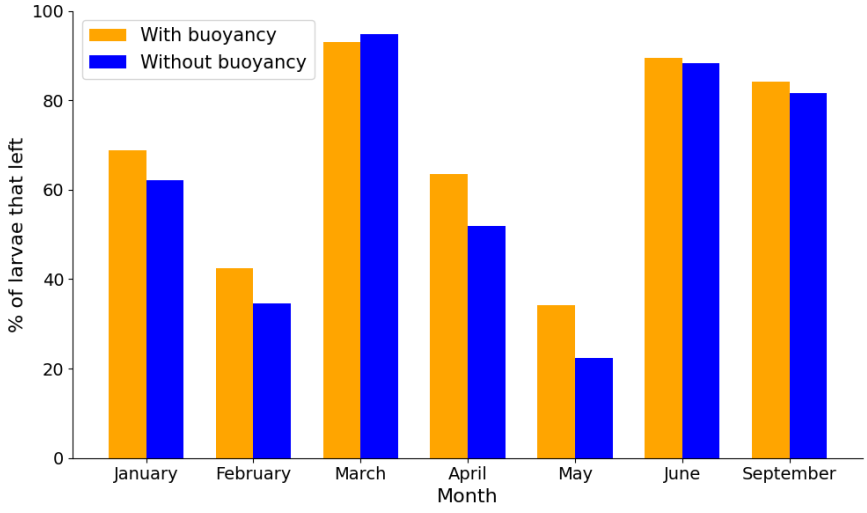

Figure 33 Percentage of larvae leaving the MP with and without positive buoyancy during the first 27 hours

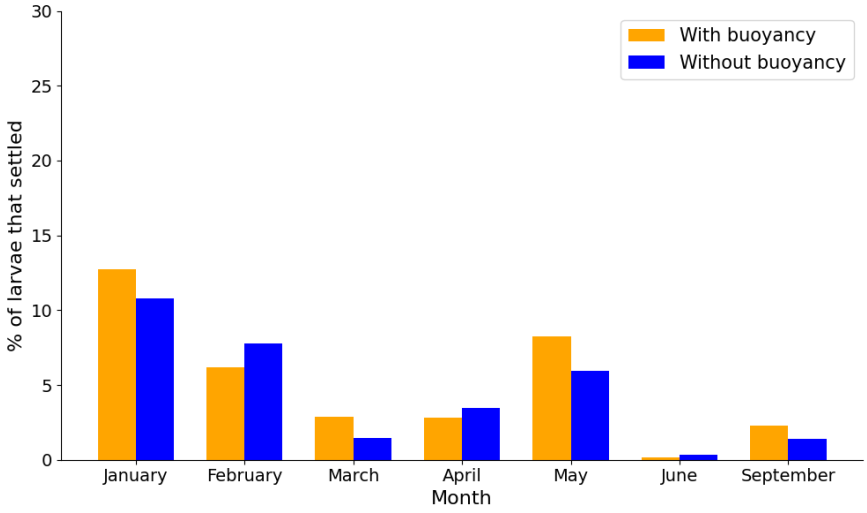

Figure 34 Percentage of larvae settling with and without a positive buoyancy during the first 27 hours

3.2.3 Connectivity of the current MPA network

Firstly, we spawned and let larvae settle only on MPAs to establish the current connectivity existing between them, while still having larvae be capable of swimming actively towards reefs and seagrass patches. For ease of use, the distinction between Marine national parks and Special reserves will not be made and MPAs will only be referred to with their name. The probability of exchange (ie. the likelihood of larvae to move from one reef to another) was computed for all seven months simulated with SLIM3D by dividing the connectivity matrix by the number of larvae seeded on each reef. MPAs are seen to be already connected through exchanges of fish larvae. The highest probabilities of exchange are observed from Curieuse (Fig. 35, MPA 0) and the Ile Coco (MPA 6) and from Port Launay (MPA 3) and Baie Launay (MPA 7) with respectively 2.1 and 2.8%. The mean probability of exchange between all MPAs is 0.47%.

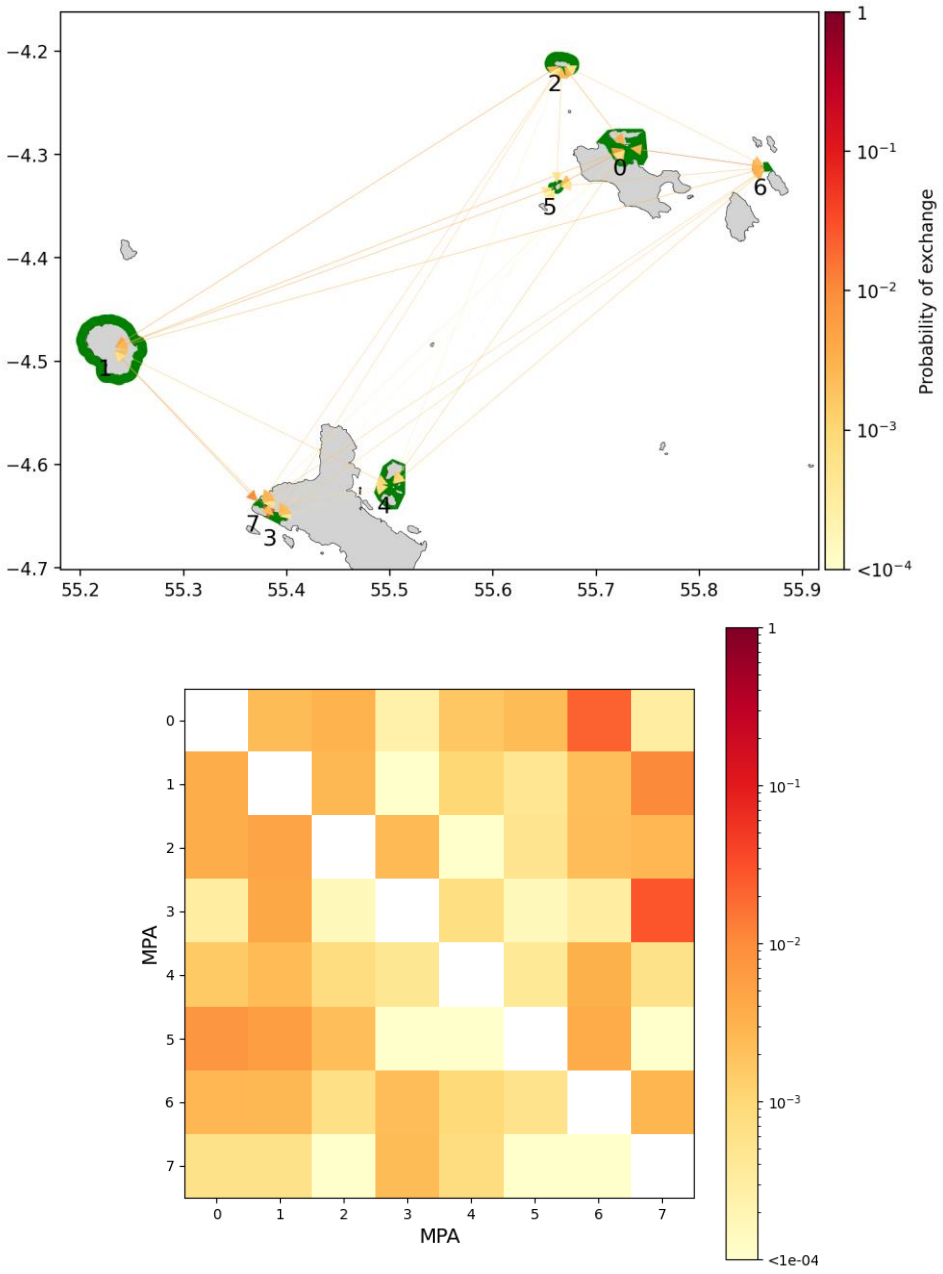

Figure 35 Probability of exchange between MPAs and associated matrix. MPAs are numbered as follow : (0) Curieuse (1) Silhouette (2) Aride (3) Port Launay (4) St. Anne (5) Cousin (6) Ile Coco (7) Baie Ternay

With the connectivity matrix built during larvae dispersal, we computed connectivity indicators for each MPA : the weighted connectivity length (WCL), the self-recruitment (SR), the proportion of larvae settled and the local retention (LR) (Fig. 36). The proportion of settled larvae is lower than 5% for most MPAs and is the highest in Baie Launay which also has the highest percentage of local retention (Fig. 36, d). WCL values of MPAs range from 1 to 48 km. The WCLs of Port Launay and Baie Ternay are the lowest (<10km) as they mostly provide larvae to each other and themselves.

Two groups of MPAs seem to appear : (1) Silhouette, St. Anne, Port Launay, Baie Ternay and (2) Cousin, Curieuse, Aride and Ile Coco with exchanges between the two groups being provided by the MPAs with WCLs higher than 30km. The self-recruitment of St. Anne and Curieuse is the highest (55%) which means they are more isolated than other MPAs.

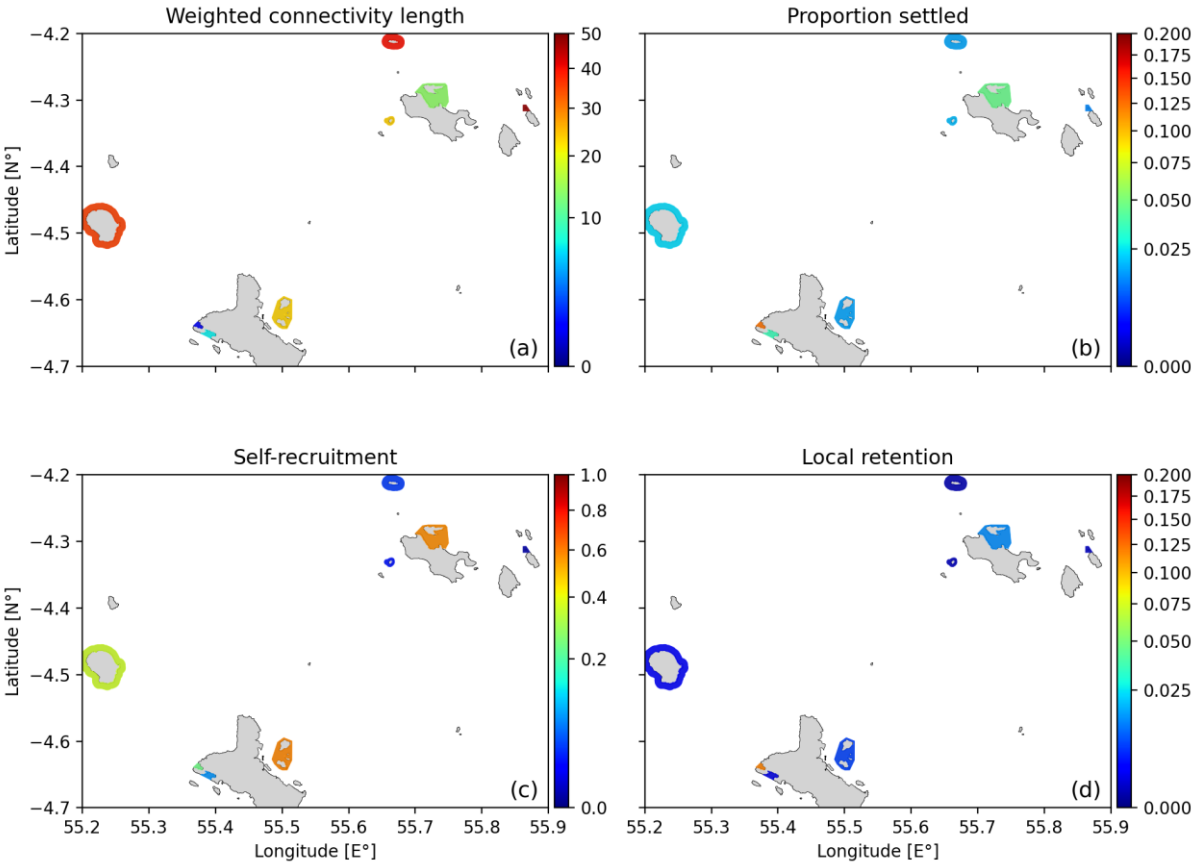

Figure 36 Connectivity indicators of MPAs : WCL (a), proportion of larvae settled (b), self-recruitment (c), local retention (d)

3.2.4 Connectivity among individual reefs

Snapper larvae swim around the MP from reef to reef creating connections between reefs in and out of MPAs. In this part, those connections are analyzed through the use of connectivity indicators.

The out-degree (OD) is based on the non-normalized connectivity matrix and reflects the out-going connections of a reef. ODs range from 0 to 93 (Fig. 37). Reefs located on the coast of Mahé island have the highest ODs of the plateau. Small outer reefs (b and c) located around 100 km away from the inner islands also present ODs ranging from 10 to 20.

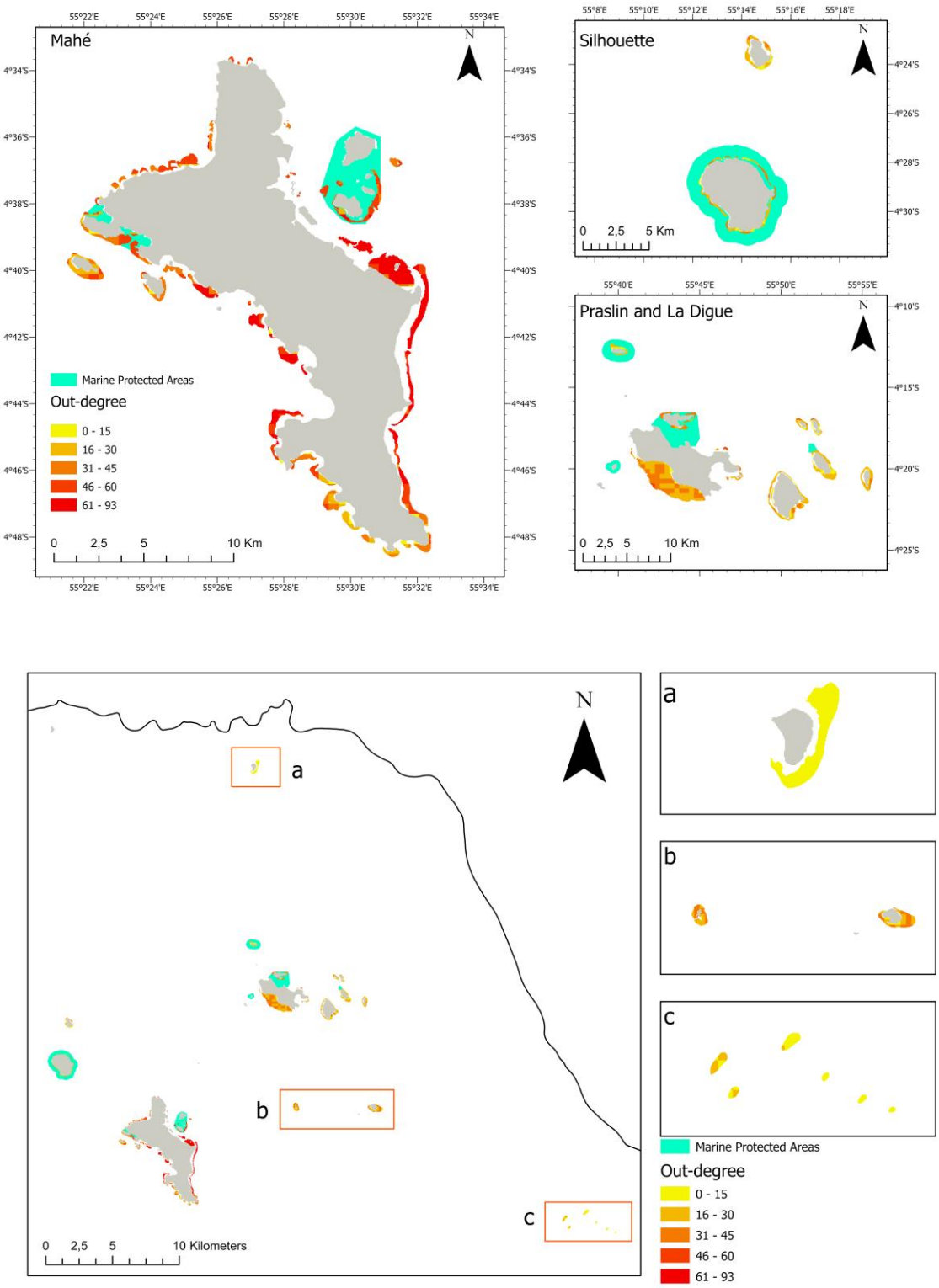

Figure 37 Out-degree of the outer reefs and reefs located around the inner islands obtained by intersecting the 500x500m squared reefs with UNEP polygons

The in-degree (ID) illustrates the incoming connections of a reef or a seagrass patch and can reach a value of 440 around Mahé. Main destinations of settling larvae are located around the inner islands (Fig. 38) while outer reefs have a non-existent ID. It is notable that important destinations of larvae are already located in MPAs, namely Silhouette, Baie Ternay, Curieuse and Aride.

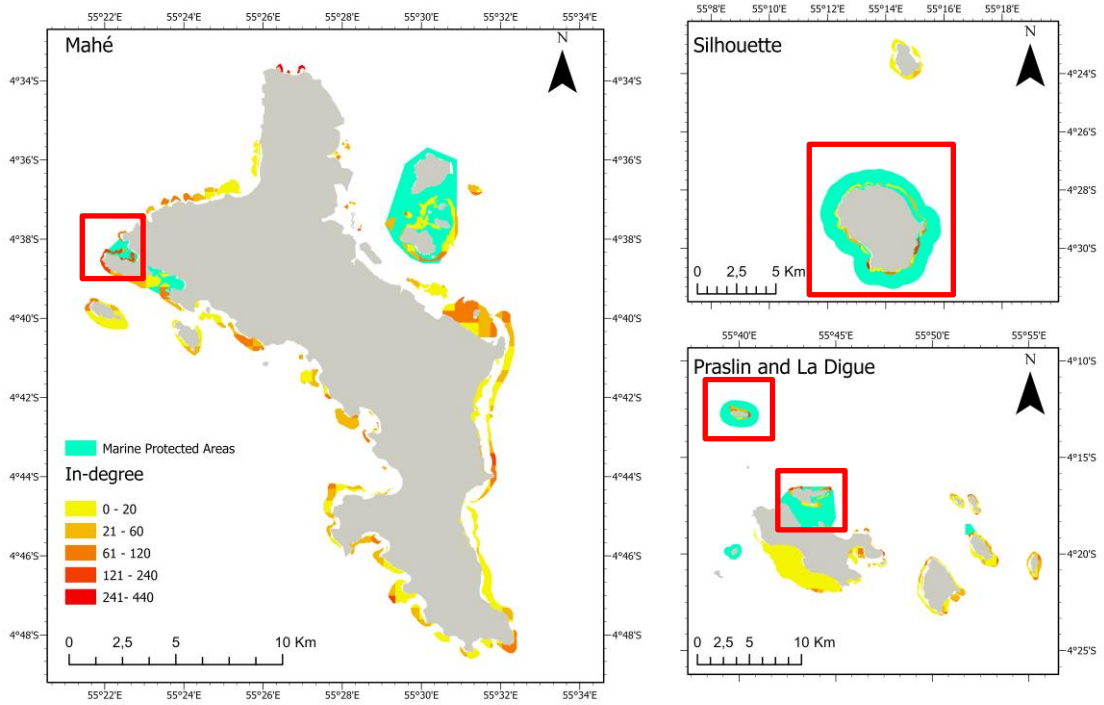

Figure 38 In-degree of the squared reefs and seagrass patches located around the inner islands obtained by intersecting the 500x500m squared reefs with UNEP polygons. Red squares highlight reefs located in MPAs and having a high- in-degree (>100)

The movement of fish larvae forms a tight network between the inner islands. Those connections change through the season and are influenced by the directions of the currents. In April, when currents have been seen to flow towards the northwest, connections between Mahé and Praslin have little to no probability of happening in contrary to connections From Mahé to Silhouette (Fig. 39). When currents are westward, in September, outer reefs supply the inner islands at a higher rate. Connections between Praslin and Mahé have a higher probability of happening in February when current flow towards the north-east. The reefs located around the island of Mahé supply each other during the entire year. Seagrass patches have an average in-degree of 22.42 while reefs have an average in-degree of 33.41.

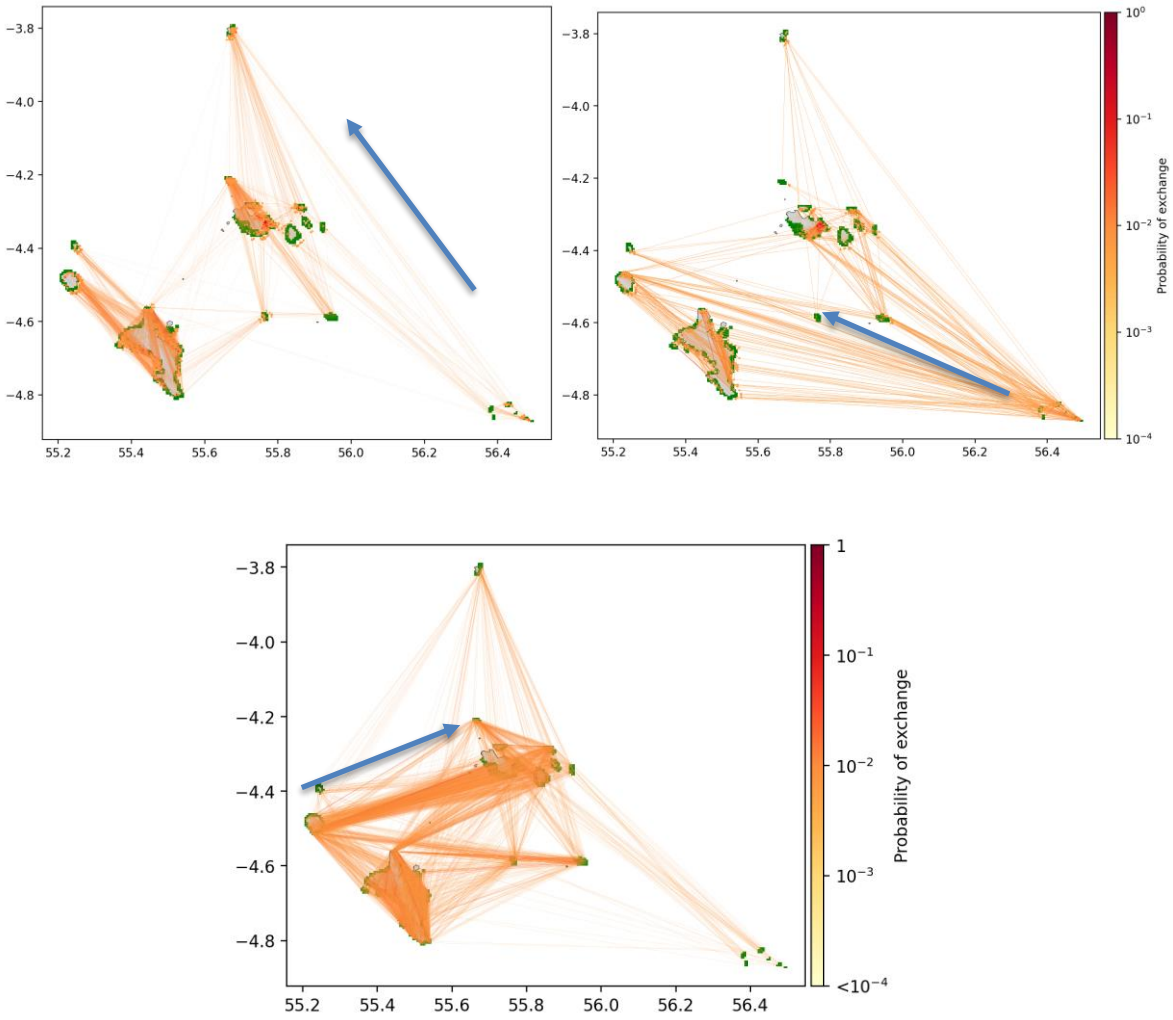

Figure 39 Probability of exchange between the reefs in April (left), September (right) and February (bottom) and main direction of connections (blue arrow)

We compute four indicators based on the connectivity matrices between reefs : the WCL, the SR, the proportion of larvae settled and the LR. It appears that the reefs north of Mahé, while having high ODs, have the lowest WCLs which are generally around 20 km (Fig. 40). Those reefs mainly export larvae to other reefs on the coast of Mahé. Reefs around Silhouette have WCL values around 60km as they export larvae to MPAs located around Praslin. Outer reefs have the highest WCL (115km). However, even if larvae from offshore reefs reach the inner islands, connections that cover distances greater than 60km form only 5% of all connections observed in the simulations and the mean WCL for all reefs is 28km. SR and LR are generally low on all reefs around the plateau. Self-recruitment peaks at 10% on reefs of the southern coast of Mahé. The proportion of larvae settled is higher around Mahé where it is on average 10%.

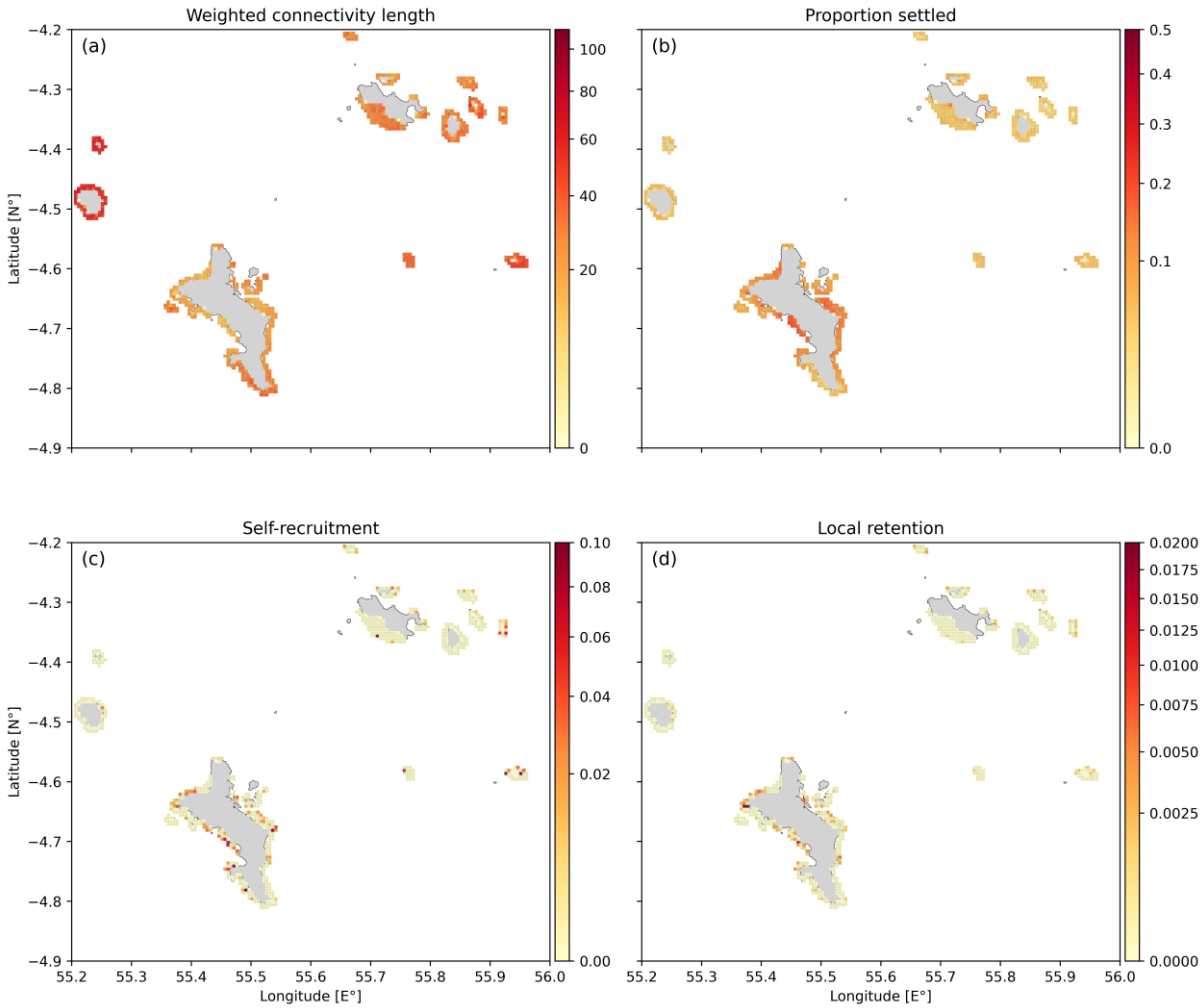

Figure 40 Connectivity indicators computer of the inner islands reefs (500x500m squared entities)

4. Discussion

In this section, we discuss the results of the hydrodynamic simulation as well as the results obtained with the Lagrangian particle tracker.

4.1 Hydrodynamics

As explained in the previous sections, the current velocity and direction of SLIM3D generally follow observed currents measured at the validation point (ADCP-E). However, the simulation does not record all variations in current velocity and direction which can happen over the course of a few days. This might be due to the lack of an atmospheric model with a spatial resolution finer than the global ERA-5 dataset, which uses a grid with a 31 km resolution

Currents modeled during each month (Fig. 24) seem to follow the pattern observed by Castillo-Trujillo et al. (2021) and Hanuise (2022) with currents flowing towards the northeast in January, February and March. Currents in May, June and September seem however to have a stronger westward component. Variations in temperature modelled by SLIM3D follow the trend observed by Castillo-Trujillo et al. (2021) with peaks in April and Mays (>29°C) and lower temperatures at the end of June (<25°C).

4.2 Larvae dispersal

This study highlights the current connectivity between Marine Protected Areas located on the Mahé plateau as well as the connectivity between reefs.

Firstly, we demonstrated that current velocity and direction impact the propagation of larvae. The monthly rate of larvae leaving the plateau was especially high (>90%) in March, June, and September. This could be due to the north-westward currents in June and September and higher surface current velocity in March. High rates of particles being carried out of the Mahé Plateau were also observed by Hanuise (2022) while studying the propagation of seagrass fragments.

The amount of larvae leaving the MP was shown to be influenced by buoyancy and lowered by 2 to 10% when no buoyant stage was considered except in March when it rose by 2%. Buoyancy showed a variable impact on the rate of larvae settling: in four months out of seven (January, March, May and September), a buoyant stage led to a rise in settling larvae while it lead to smaller settling rates in February, April and June. Buoyancy of fish eggs has, however, been seen to lower settling rates in other studies. For example, in the case of the Lutjanus campechanus in the Gulf of Mexico, successful settling rates dropped by 20% when adding a buoyant stage to passive larvae (Zhou et al. 2024). Buoyancy has been seen to raise dispersal lengths (Leis 2020) which could explain why larvae leave the

plateau at a higher percentage with a buoyant stage. The dispersion of larvae from the Seychelles archipelago at the scale of the Western Indian Ocean has also been observed by Gamoyo, Obura, and Reason (2019) who showed that passive larvae spawned by reefs on the Mahé plateau spread at distances of 101 ± 63 km which could correlate with the high percentage of larvae leaving the MP in our simulations.

Secondly, the connectivity study of MPAs showed that the probability of exchange between MPAs was at most 2.8% and 0.47% on average. Probability of exchanges obtained here are in line with what was observed by Burt et al. (2024) in a connectivity analysis of the islands of the Seychelles archipelago through the movement of coral larvae and which found a transport probability between the inner islands of $\sim 10^{-3}$. Results were however lower when considering the probability of exchange between all reefs which was, on average, $8*10^{-5}$.

Considering all reefs, we found that connections between reefs were mainly at distances less than 60 km, resulting in a deeply intertwined network around the inner islands of the MP. In those simulations, connections from outer reefs to the inner islands represented less than 5% of all connections. This does not mean however that outer reefs should not be considered as potential sources or sinks of larvae as only nine individual outer reefs were considered in those simulations and actual sources of larvae are not known.

The monthly variations in connectivity patterns highlight that larvae dispersal on the MP is highly influenced by monthly currents. For example, in April, northwest currents reduce connectivity between Mahé and Praslin, while September's westward currents enhance connections from outer reefs to inner islands. Similar results were obtained by Vogt-Vincent, Mitarai, and Johnson (2023) for coral dispersal in the tropical southwest Indian Ocean which highlighted the variation of connectivity on a week to week and even daily basis.

Finally, potential gaps in the current MPA network would depend on the goal of the chosen MPA. Reefs that have a higher out-degree and settling rate but a low WCL, like seen on the coast of Mahé Island, have the potential to supply larvae to other reefs or seagrass patches which are also located on Mahé island. Reefs with a high out-degree and a high WCL, like seen north of Silhouette, on the other hand would favor longer-distance dispersal. The in-degree showed key destinations of larvae around the inner islands, with some already being part of MPAs, which could provide protection to fishes having just finished their pelagic larval stage.

However, this study has limitations. Larval dispersion is a complex process and the results of this study are dependent on chosen model parameters and larvae behaviors. A potential vertical ontogenetic migration process, which can entail daily movement of the larvae from and to the bottom of the ocean as well as vertical movements following food sources like phytoplankton was not taken into account and has been seen to have a positive impact on settling rates (Hernández et al. 2023; Zhou et al. 2024). Model parameters such as main life stages were also based on the Letjanus campechanus which, while being in the same genus, might not fully apply to the Lutjanus sebae. Assumptions were also made about the potential spawning and settling grounds which at this time, are not known.

Another limitation of this study is the length of the simulations which only last seven months and are not expected to be a fully accurate representation of ocean circulation on the Mahé plateau. This could explain the difference with results obtained by Castillo-Trujillo et al. (2021) which were computed between 1993 and 2009. This time period also did not allow for a full exploration of the dispersal dynamics of fish larvae as the ocean circulation of the plateau is highly dependent on the northern and southern monsoons. Longer simulation periods might be necessary to develop a better understanding of the larvae dispersal around the plateau. However, the use of a 3D model did however allow for an exploration of the impacts of vertical movements lead by water currents and buoyancy but did cause a diminishing in horizontal resolution as modelling the full 3D ocean circulation is more computationally heavy than modelling 2D currents.

Connectivity is also not the only criterion to be taken into account while planning the creation of an MPA network and not an end in itself. According to the IUCN (Laffoley 2008), MPAn should, for example, take into consideration the economic and social situation of their location, as they can impose a financial and social burden on local populations. As previously stated, connectivity is also only part of one guideline out of five set by the IUCN in 2008 for the design of resilient MPA network which should also include: (1) a variety in habitats to represent all ecosystems and habitats in the region (2) ecologically significant areas like nurseries or spawning aggregations (3) long-term protection (4) the maximum contribution of individual MPAs to the network.

5. Conclusion

MPAs are a common tool used worldwide to enhance the protection of marine biodiversity and have begun to include the question of connectivity in their creation with the goal to improve the movements of marine species from and to MPAs thereby enhancing the diversity and stability of marine populations. In this study, we tried to investigate the current connectivity of MPAs located on the MP in the Seychelles archipelago and identify potential locations of MPAs.

The first step to estimate movements of fish larvae around the MP was to simulate the hydrodynamics of the area using SLIM3D over a seven-month period (January to June and September 2018). The output of SLIM3D was then coupled with a LPT to simulate the movement of fish larvae around the plateau. Simulations were done by dividing the life of the fish larvae into five main stages : egg, pre-flexion, notochord flexion, post flexion and settling between 26 and 30 days of age. Connectivity indicators were then used to investigate the connections between reefs and MPAs.

This modelling approach allows us to answer the questions set at the beginning of this study : how can we characterize the connectivity between reefs on the Mahé plateau and how do MPAs contribute to the dispersal of larvae? Are there any gaps in the current MPA network?

Results suggest than the connectivity between reefs and MPAs of the MP is highly influenced by the direction and velocity of the currents which varies from month to month and impacts the amount of larvae leaving the MP as well as settling on reefs. Settling rates reached a peak in January with 12.5% but were seen to be really low in months with north-westward currents like in June. Outer reefs located east of the inner islands have the potential to supply them with larvae, however their probability of exchange is highly dependent on westward currents.

Currently, two groups of MPAs seem to appear, one around Mahé and Silhouette and the other around Praslin and La Digue. Exchanges between these two groups are provided by the MPAs with WCLs higher than 30km, namely the Silhouette Marine national park and the Aride special reserve. Other MPAs mainly exchange larvae with MPAs closer than 30km.

Connectivity between reefs has the potential to influence the implementation of new MPAs by favoring reefs with the chosen characteristics. Reefs with high IDs and ODs, especially around Mahé could be could suppliers and receivers of larvae however, their impact is mostly limited to other reefs located around the island or themselves which is seen through their higher local retention and higher weighted connectivity lengths. Reefs around Praslin, while having lower in-degrees, could be good suppliers of larvae to other reefs.

It is notable that important destinations of larvae are already located in MPAs, namely the Silhouette Marine National Park, the Baie Ternay Marine National Park, the Curieuse Marine National Park and the Aride Special Reserve as seen through their higher in-degrees.

The results of this study could be improved with better data on larvae behavior as well as longer simulation periods. However, they offer insight on the connectivity of reefs located on the Mahé plateau and the potential dynamic of larvae exchanges which could offer important data for the potential implementation of new MPAs . The good results obtained with SLIM3D also show its potential, especially in this region.

Bibliography

Advance Africa Management Services. 2015. *Seychelles Mariculture Master Plan: Aquaculture Fact Sheet - Emperor, Red Snapper Lutjanus Sebae*.

Airamé, Satie, Jenifer E. Dugan, Kevin D. Lafferty, Heather Leslie, Deborah A. McArdle, and Robert R. Warner. 2003. "APPLYING ECOLOGICAL CRITERIA TO MARINE RESERVE DESIGN: A CASE STUDY FROM THE CALIFORNIA CHANNEL ISLANDS." *Ecological Applications* 13(sp1): 170–84. doi:10.1890/1051-0761(2003)013[0170:AECTMR]2.0.CO;2.

Alaerts, Lauranne. 2021. "Evaluation of the Impacts of Climate Change on the Distribution of Florida Stone Crab Larvae on the West Florida Shelf. Prom. : Hanert, Emmanuel." Faculté des bioingénieurs, Université catholique de Louvain,. http://hdl.handle.net/2078.1/thesis:30416.

Alaerts, Lauranne, Thomas Dobbelaere, Philip M. Gravinese, and Emmanuel Hanert. 2022. "Climate Change Will Fragment Florida Stone Crab Communities." *Frontiers in Marine Science* 9: 839767. doi:10.3389/fmars.2022.839767.

Allen, G.R. 1985. *FAO Species Catalogue. Vol. 6. Snappers of the World. AN Annotated and Illustrated Catalogue of Lutjanid Species Known to Date.* Rome: FAO.

Anadón, José D, Maria Del Mar Mancha-Cisneros, Benjamin D Best, and Leah R Gerber. 2013. "Habitat-specific Larval Dispersal and Marine Connectivity: Implications for Spatial Conservation Planning." *Ecosphere* 4(7): 1–15. doi:10.1890/ES13-00119.1.

AquaMaps. 2019. "Computer Generated Distribution Maps for Lutjanus Sebae (Emperor Red Snapper), with Modelled Year 2050 Native Range Map Based on IPCC RCP8.5 Emissions Scenario." https://www.aquamaps.org.

Assis, Jorge, Pierre Failler, Eliza Fragkopoulou, David Abecasis, Gregoire Touron-Gardic, Aissa Regalla, Ebaye Sidina, Herculano Dinis, and Ester A. Serrao. 2021. "Potential Biodiversity Connectivity in the Network of Marine Protected Areas in Western Africa." *Frontiers in Marine Science* 8: 765053. doi:10.3389/fmars.2021.765053.

Babcock, R. C., N. T. Shears, A. C. Alcala, N. S. Barrett, G. J. Edgar, K. D. Lafferty, T. R. McClanahan, and G. R. Russ. 2010. "Decadal Trends in Marine Reserves Reveal Differential Rates of Change in Direct and Indirect Effects." *Proceedings of the National Academy of Sciences* 107(43): 18256–61. doi:10.1073/pnas.0908012107.

Balbar, Arieanna C., and Anna Metaxas. 2019. "The Current Application of Ecological Connectivity in the Design of Marine Protected Areas." *Global Ecology and Conservation* 17: e00569. doi:10.1016/j.gecco.2019.e00569.

Ball, I.R., H.P. Possingham, and M. Watts. 2009. "Marxan and Relatives: Software for Spatial Conservation Proritisation." In *Spatial Conservation Prioritisation :*

Quantative Methods and Computational Tools., Oxford, UK: Oxford University Press, 185–95.

Berkström, Charlotte, Lovisa Wennerström, and Ulf Bergström. 2022. "Ecological Connectivity of the Marine Protected Area Network in the Baltic Sea, Kattegat and Skagerrak: Current Knowledge and Management Needs." *Ambio* 51(6): 1485–1503. doi:10.1007/s13280-021-01684-x.

Bourque, Bradford D., and Ronald P. Phelps. 2007. "Induced Spawning and Egg Quality Evaluation of Red Snapper, *Lutjanus Campechanus*." *Journal of the World Aquaculture Society* 38(2): 208–17. doi:10.1111/j.1749-7345.2007.00090.x.

Burt, April J., Noam Vogt-Vincent, Helen Johnson, Ashley Sendell-Price, Steve Kelly, Sonya M. Clegg, Catherine Head, et al. 2024. "Integration of Population Genetics with Oceanographic Models Reveals Strong Connectivity among Coral Reefs across Seychelles." *Scientific Reports* 14(1): 4936. doi:10.1038/s41598-024-55459-x.

Calvin, Katherine, Dipak Dasgupta, Gerhard Krinner, Aditi Mukherji, Peter W. Thorne, Christopher Trisos, José Romero, et al. 2023. *IPCC, 2023: Climate Change 2023: Synthesis Report. Contribution of Working Groups I, II and III to the Sixth Assessment Report of the Intergovernmental Panel on Climate Change [Core Writing Team, H. Lee and J. Romero (Eds.)]. IPCC, Geneva, Switzerland.* First. Intergovernmental Panel on Climate Change (IPCC). doi:10.59327/IPCC/AR6-9789291691647.

Carr, Mark H., Sarah P. Robinson, Charles Wahle, Gary Davis, Stephen Kroll, Samantha Murray, Ervin Joe Schumacker, and Margaret Williams. 2017. "The Central Importance of Ecological Spatial Connectivity to Effective Coastal Marine Protected Areas and to Meeting the Challenges of Climate Change in the Marine Environment." *Aquatic Conservation: Marine and Freshwater Ecosystems* 27(S1): 6–29. doi:10.1002/aqc.2800.

Castillo-Trujillo, Alma Carolina, Isabella B. Arzeno-Soltero, Sarah N. Giddings, Geno Pawlak, Julie McClean, and Luc Rainville. 2021. "Observations and Modeling of Ocean Circulation in the Seychelles Plateau Region." *Journal of Geophysical Research: Oceans* 126(2): e2020JC016593. doi:10.1029/2020JC016593.

Cheung, William W. L., Jorge L. Sarmiento, John Dunne, Thomas L. Frölicher, Vicky W. Y. Lam, M. L. Deng Palomares, Reg Watson, and Daniel Pauly. 2013. "Shrinking of Fishes Exacerbates Impacts of Global Ocean Changes on Marine Ecosystems." *Nature Climate Change* 3(3): 254–58. doi:10.1038/nclimate1691.

Cheung, William W.L., Vicky W.Y. Lam, Jorge L. Sarmiento, Kelly Kearney, Reg Watson, and Daniel Pauly. 2009. "Projecting Global Marine Biodiversity Impacts under Climate Change Scenarios." *Fish and Fisheries* 10(3): 235–51. doi:10.1111/j.1467-2979.2008.00315.x.

Coleman, Felicia C., and Susan L. Williams. 2002. "Overexploiting Marine Ecosystem Engineers: Potential Consequences for Biodiversity." *Trends in Ecology & Evolution* 17(1): 40–44. doi:10.1016/S0169-5347(01)02330-8.

Connell, Sean D., and Bronwyn M. Gillanders, eds. 2007. *Marine Ecology*. South Melbourne, Vic: Oxford University Press.

Daigle, Rémi M., Anna Metaxas, Arieanna C. Balbar, Jennifer McGowan, Eric A. Treml, Caitlin D. Kuempel, Hugh P. Possingham, and Maria Beger. 2020. "Operationalizing Ecological Connectivity in Spatial Conservation Planning with Marxan Connect" ed. Nick Golding. *Methods in Ecology and Evolution* 11(4): 570–79. doi:10.1111/2041-210X.13349.

Dobbelaere, Thomas, Erinn M. Muller, Lewis J. Gramer, Daniel M. Holstein, and Emmanuel Hanert. 2020. "Coupled Epidemio-Hydrodynamic Modeling to Understand the Spread of a Deadly Coral Disease in Florida." *Frontiers in Marine Science* 7: 591881. doi:10.3389/fmars.2020.591881.

Doney, Scott C., Victoria J. Fabry, Richard A. Feely, and Joan A. Kleypas. 2009. "Ocean Acidification: The Other CO 2 Problem." *Annual Review of Marine Science* 1(1): 169–92. doi:10.1146/annurev.marine.010908.163834.

Drass, Denice, Kevin Bootes, Joanne Lyczkowski-Shultz, Bruce Comyns, Gloria Holt, Cecilia Riley, and Ronald Phelps. 2000. "Larval Development of Red Snapper, Lutjanus Campechanus, and Comparisons with Co-Occurring Snapper Species." 98: 507–27.

Dudley, Nigel, and Sue Stolton. 2008. *Defining Protected Areas: An International Conference in Almeria*. Gland, Switzerland: IUCN.

Ecosystems and Human Well-Being: Biodiversity Synthesis. 2005. Washington, DC: World Resources Institute. Millennium Ecosystem Assessment.

Edgar, Graham J., Rick D. Stuart-Smith, Trevor J. Willis, Stuart Kininmonth, Susan C. Baker, Stuart Banks, Neville S. Barrett, et al. 2014. "Global Conservation Outcomes Depend on Marine Protected Areas with Five Key Features." *Nature* 506(7487): 216–20. doi:10.1038/nature13022.

Egbert, Gary D., and Svetlana Y. Erofeeva. 2002. "Efficient Inverse Modeling of Barotropic Ocean Tides." *Journal of Atmospheric and Oceanic Technology* 19(2): 183–204. doi:10.1175/1520-0426(2002)019<0183:EIMOBO>2.0.CO;2.

European Union-Copernicus Marine Service. 2015. "Global Ocean OSTIA Sea Surface Temperature and Sea Ice Analysis." doi:10.48670/MOI-00165.

FAO, ed. 2022. *Towards Blue Transformation*. Rome: FAO. doi:10.4060/cc0461en.

Fisher, Rebecca, Jeffrey M. Leis, Domine L. Clark, and Shaun K. Wilson. 2005. "Critical Swimming Speeds of Late-Stage Coral Reef Fish Larvae: Variation within Species, among Species and between Locations." *Marine Biology* 147(5): 1201–12. doi:10.1007/s00227-005-0001-x.

Friesen, Sarah K., Rebecca Martone, Emily Rubidge, Jacopo A. Baggio, and Natalie C. Ban. 2019. "An Approach to Incorporating Inferred Connectivity of Adult Movement

into Marine Protected Area Design with Limited Data." *Ecological Applications* 29(4): e01890. doi:10.1002/eap.1890.

Frys, Charles, Antoine Saint-Amand, Matthieu Le Hénaff, Joana Figueiredo, Alyson Kuba, Brian Walker, Jonathan Lambrechts, et al. 2020. "Fine-Scale Coral Connectivity Pathways in the Florida Reef Tract: Implications for Conservation and Restoration." *Frontiers in Marine Science* 7: 312. doi:10.3389/fmars.2020.00312.

Galpern, Paul, Micheline Manseau, and Andrew Fall. 2011. "Patch-Based Graphs of Landscape Connectivity: A Guide to Construction, Analysis and Application for Conservation." *Biological Conservation* 144(1): 44–55. doi:10.1016/j.biocon.2010.09.002.

Gamoyo, Majambo, David Obura, and Chris J. C. Reason. 2019. "Estimating Connectivity Through Larval Dispersal in the Western Indian Ocean." *Journal of Geophysical Research: Biogeosciences* 124(8): 2446–59. doi:10.1029/2019JG005128.

Gill, David A., Michael B. Mascia, Gabby N. Ahmadia, Louise Glew, Sarah E. Lester, Megan Barnes, Ian Craigie, et al. 2017. "Capacity Shortfalls Hinder the Performance of Marine Protected Areas Globally." *Nature* 543(7647): 665–69. doi:10.1038/nature21708.

GOS. 2014. *Seychelles Biodiversity Strategy and Action Plan 2015-2020*.

Grandcourt, E. M., T. Hecht, A. J. Booth, and J. Robinson. 2008. "Retrospective Stock Assessment of the Emperor Red Snapper (Lutjanus Sebae) on the Seychelles Bank between 1977 and 2006." *ICES Journal of Marine Science* 65(6): 889–98. doi:10.1093/icesjms/fsn064.

Gräwe, Ulf, and Jörg-Olaf Wolff. 2010. "Suspended Particulate Matter Dynamics in a Particle Framework." *Environmental Fluid Mechanics* 10(1–2): 21–39. doi:10.1007/s10652-009-9141-8.

Green, Alison, Scott E. Smith, Geoff Lipsett-Moore, Craig Groves, Nate Peterson, Stu Sheppard, Paul Lokani, et al. 2009. "Designing a Resilient Network of Marine Protected Areas for Kimbe Bay, Papua New Guinea." *Oryx* 43(4): 488–98. doi:10.1017/S0030605309990342.

Grorud-Colvert, Kirsten, Jenna Sullivan-Stack, Callum Roberts, Vanessa Constant, Barbara Horta E Costa, Elizabeth P. Pike, Naomi Kingston, et al. 2021. "The MPA Guide: A Framework to Achieve Global Goals for the Ocean." *Science* 373(6560): eabf0861. doi:10.1126/science.abf0861.

Gruber, Nicolas, Dominic Clement, Brendan R. Carter, Richard A. Feely, Steven Van Heuven, Mario Hoppema, Masao Ishii, et al. 2019. "The Oceanic Sink for Anthropogenic CO_2 from 1994 to 2007." *Science* 363(6432): 1193–99. doi:10.1126/science.aau5153.

Guinotte, John M., and Victoria J. Fabry. 2008. "Ocean Acidification and Its Potential Effects on Marine Ecosystems." *Annals of the New York Academy of Sciences* 1134(1): 320–42. doi:10.1196/annals.1439.013.

Hannesson, R. 2013. “Exclusive Economic Zone.” In *Encyclopedia of Energy, Natural Resource, and Environmental Economics*, Elsevier, 150–53. doi:10.1016/B978-0-12-375067-9.00046-2.

Hanuise, Douchan. 2022. “Investigating the Contribution of Seychelles’ Seagrass Meadows to Marine Carbon Sequestration.” Faculté des bioingénieurs, Université catholique de Louvain. http://hdl.handle.net/2078.1/thesis:35800.

Harley, Christopher D. G., A. Randall Hughes, Kristin M. Hultgren, Benjamin G. Miner, Cascade J. B. Sorte, Carol S. Thornber, Laura F. Rodriguez, Lars Tomanek, and Susan L. Williams. 2006. “The Impacts of Climate Change in Coastal Marine Systems.” *Ecology Letters* 9(2): 228–41. doi:10.1111/j.1461-0248.2005.00871.x.

Heck, Kenneth L., Tim J. B. Carruthers, Carlos M. Duarte, A. Randall Hughes, Gary Kendrick, Robert J. Orth, and Susan W. Williams. 2008. “Trophic Transfers from Seagrass Meadows Subsidize Diverse Marine and Terrestrial Consumers.” *Ecosystems* 11(7): 1198–1210. doi:10.1007/s10021-008-9155-y.

Hernández, Christina M., Claire B. Paris, Ana C. Vaz, Benjamin T. Jones, Julie B. Kellner, David E. Richardson, Su Sponaugle, Robert K. Cowen, and Joel K. Llopiz. 2023. “Diverse Patterns of Larval Coral Reef Fish Vertical Distribution and Consequences for Dispersal and Connectivity.” *Coral Reefs* 42(2): 453–65. doi:10.1007/s00338-023-02355-x.

Kinlan, Brian P., and Steven D. Gaines. 2003. “PROPAGULE DISPERSAL IN MARINE AND TERRESTRIAL ENVIRONMENTS: A COMMUNITY PERSPECTIVE.” *Ecology* 84(8): 2007–20. doi:10.1890/01-0622.

Kroeker, Kristy J., Rebecca L. Kordas, Ryan Crim, Iris E. Hendriks, Laura Ramajo, Gerald S. Singh, Carlos M. Duarte, and Jean-Pierre Gattuso. 2013. “Impacts of Ocean Acidification on Marine Organisms: Quantifying Sensitivities and Interaction with Warming.” *Global Change Biology* 19(6): 1884–96. doi:10.1111/gcb.12179.

Laffoley, Daniel D’A. 2008. *Establishing Resilient Marine Protected Area Networks--Making It Happen: Full Technical Version, Including Ecological, Social and Governance Considerations, as Well as Case Studies*. Washington, D.C.: IUCN-WCPA : National Oceanic and Atmospheric Association : The Nature Conservancy.

Lam, Vicky W. Y., William W. L. Cheung, Gabriel Reygondeau, and U. Rashid Sumaila. 2016. “Projected Change in Global Fisheries Revenues under Climate Change.” *Scientific Reports* 6(1): 32607. doi:10.1038/srep32607.

Leis, Jeffrey M. 2020. “Perspectives on Larval Behaviour in Biophysical Modelling of Larval Dispersal in Marine, Demersal Fishes.” *Oceans* 2(1): 1–25. doi:10.3390/oceans2010001.

Lowe, Winsor H., and Fred W. Allendorf. 2010. “What Can Genetics Tell Us about Population Connectivity?: GENETIC AND DEMOGRAPHIC CONNECTIVITY.” *Molecular Ecology* 19(15): 3038–51. doi:10.1111/j.1365-294X.2010.04688.x.

Lyons, Mitchell, Kirk Larsen, and Matt Skone. 2022. “CoralMapping/AllenCoralAtlas: DOI for Paper at ~ v1.3.” doi:10.5281/ZENODO.3833242.

Madec, Gurvan, Mike Bell, Adam Blaker, Clément Bricaud, Diego Bruciaferri, Miguel Castrillo, Daley Calvert, et al. 2023. “NEMO Ocean Engine Reference Manual.” doi:10.5281/ZENODO.8167700.

McClanahan, Timothy R., Michael J. Marnane, Joshua E. Cinner, and William E. Kiene. 2006. “A Comparison of Marine Protected Areas and Alternative Approaches to Coral-Reef Management.” *Current Biology* 16(14): 1408–13. doi:10.1016/j.cub.2006.05.062.

Nellemann, C. and GRID--Arendal, eds. 2009. *Blue Carbon: The Role of Healthy Oceans in Binding Carbon: A Rapid Response Assessment*. Arendal, [Norway]: GRID-Arendal.

Okubo, Akira. 1971. “Oceanic Diffusion Diagrams.” *Deep Sea Research and Oceanographic Abstracts* 18(8): 789–802. doi:10.1016/0011-7471(71)90046-5.

Orth, Robert J., Tim J. B. Carruthers, William C. Dennison, Carlos M. Duarte, James W. Fourqurean, Kenneth L. Heck, A. Randall Hughes, et al. 2006. “A Global Crisis for Seagrass Ecosystems.” *BioScience* 56(12): 987. doi:10.1641/0006-3568(2006)56[987:AGCFSE]2.0.CO;2.

Paris, Claire B., Judith Helgers, Erik Van Sebille, and Ashwanth Srinivasan. 2013. “Connectivity Modeling System: A Probabilistic Modeling Tool for the Multi-Scale Tracking of Biotic and Abiotic Variability in the Ocean.” *Environmental Modelling & Software* 42: 47–54. doi:10.1016/j.envsoft.2012.12.006.

Pinsky, Malin L., Boris Worm, Michael J. Fogarty, Jorge L. Sarmiento, and Simon A. Levin. 2013. “Marine Taxa Track Local Climate Velocities.” *Science* 341(6151): 1239–42. doi:10.1126/science.1239352.

Roberts, Callum M., Bethan C. O’Leary, Douglas J. McCauley, Philippe Maurice Cury, Carlos M. Duarte, Jane Lubchenco, Daniel Pauly, et al. 2017. “Marine Reserves Can Mitigate and Promote Adaptation to Climate Change.” *Proceedings of the National Academy of Sciences* 114(24): 6167–75. doi:10.1073/pnas.1701262114.

Scherpereel Colin. 2022. “Investigating the Transmission of the Stony Coral Tissue Loss Disease among Coral Reefs in the US Virgin Islands.” Faculté des bioingénieurs, Université Catholique de Louvain. http://hdl.handle.net/2078.1/thesis:35791.

Scripps Institution of Oceanography, Luca Centurioni, Verena Hormann, Lynne Talley, Isabella Arzeno, Lisa Beal, Michael Caruso, et al. 2017. “Northern Arabian Sea Circulation-Autonomous Research (NASCar): A Research Initiative Based on Autonomous Sensors.” *Oceanography* 30(2): 74–87. doi:10.5670/oceanog.2017.224.

“Seychelles Designates 30% of Its EEZ as Marine Protected Area.” 2020. *State House, Office of the President of the Republic of Seychelles*. https://www.statehouse.gov.sc/news/4787/seychelles-designates-30-of-its-eez-as-marine-protected-area (November 11, 2023).

"Seychelles Marine Spatial Plan Initiative." 2023. *Seychelles Marine Spatial Plan*. https://seymsp.com/the-initiative/ (November 23, 2023).

Smagorinsky, J. 1963. "GENERAL CIRCULATION EXPERIMENTS WITH THE PRIMITIVE EQUATIONS: I. THE BASIC EXPERIMENT*." *Monthly Weather Review* 91(3): 99–164. doi:10.1175/1520-0493(1963)091<0099:GCEWTP>2.3.CO;2.

Speed, Conrad W., Mike Cappo, and Mark G. Meekan. 2018. "Evidence for Rapid Recovery of Shark Populations within a Coral Reef Marine Protected Area." *Biological Conservation* 220: 308–19. doi:10.1016/j.biocon.2018.01.010.

Sundby, Svein, and Trond Kristiansen. 2015. "The Principles of Buoyancy in Marine Fish Eggs and Their Vertical Distributions across the World Oceans" ed. Steven J. Bograd. *PLOS ONE* 10(10): e0138821. doi:10.1371/journal.pone.0138821.

Treml, Eric A., Patrick N. Halpin, Dean L. Urban, and Lincoln F. Pratson. 2008. "Modeling Population Connectivity by Ocean Currents, a Graph-Theoretic Approach for Marine Conservation." *Landscape Ecology* 23(S1): 19–36. doi:10.1007/s10980-007-9138-y.

UNEP-WCMC, WorldFish, World Resources Institute, and The Nature Conservancy. 2010. "Global Distribution of Coral Reefs." : 1.33 GB. doi:10.34892/T2WK-5T34.

Urban, Dean, and Timothy Keitt. 2001. "LANDSCAPE CONNECTIVITY: A GRAPH-THEORETIC PERSPECTIVE." *Ecology* 82(5): 1205–18. doi:10.1890/0012-9658(2001)082[1205:LCAGTP]2.0.CO;2.

Vallaeys, Valentin. 2018. "Discontinuous Galerkin finite element modelling of estuarine and plume dynamics. Prom. : Deleersnijder, Eric ; Hanert, Emmanuel." Université Catholique de Louvain. http://hdl.handle.net/2078.1/203013.

Vogt-Vincent, Noam S., and Helen L. Johnson. 2023. "Multidecadal and Climatological Surface Current Simulations for the Southwestern Indian Ocean at 1/50° Resolution." *Geoscientific Model Development* 16(3): 1163–78. doi:10.5194/gmd-16-1163-2023.

Vogt-Vincent, Noam S., Satoshi Mitarai, and Helen L. Johnson. 2023. "High-frequency Variability Dominates Potential Connectivity between Remote Coral Reefs." *Limnology and Oceanography* 68(12): 2733–48. doi:10.1002/lno.12455.

Watson, James E. M., Nigel Dudley, Daniel B. Segan, and Marc Hockings. 2014. "The Performance and Potential of Protected Areas." *Nature* 515(7525): 67–73. doi:10.1038/nature13947.

Winston, J. E. 2012. "Dispersal in Marine Organisms without a Pelagic Larval Phase." *Integrative and Comparative Biology* 52(4): 447–57. doi:10.1093/icb/ics040.

Zhou, Xing, Luisa Lopera, Adela Roa-Varón, and Annalisa Bracco. 2024. "Modeling the Larval Dispersal and Connectivity of Red Snapper (Lutjanus Campechanus) in the Northern Gulf of Mexico." *Progress in Oceanography* 224: 103265. doi:10.1016/j.pocean.2024.103265.

Assessing the Response of Seychelles Fish Biodiversity to Protection Status and Seascape Conditions

Marie Jacquemin

Marine protected areas (MPAs) are a common tool used worldwide to enhance the protection of marine biodiversity. In recent years, MPAs and MPA networks have begun to include the question of connectivity, which manifests through the movement of juveniles and adults, in their creation with the goal to enhance population stability and diversity in and out of MPAs. In this study, we investigate the connectivity of the current MPA network located on the Mahé Plateau, Seychelles with the goal to identify the dispersal dynamic of fish larvae and potential gaps in the network. To do so, we use a three-dimensional ocean model, SLIM3D, over a seven-month period. We couple it with a larval dispersal model based on the behaviour of Lutjanus sebae, a key commercial and overexploited fish in the Seychelles. Larvae behaviour is divided into five main life stages : egg, pre-flexion, flexion, post-flexion and settlement. We then conduct a connectivity analysis on the MPAs and reefs located on the Mahé plateau. Our results suggest that the varying dynamic of the currents has an impact on the direction of exchanges of larvae between the inner islands and outer reefs of the plateau as well as on the percentage of settling larvae which reaches a peak in January (12.5%). We find that the probability of exchange between MPAs currently reach up to 2.8% and identify potential locations of new MPAs on reefs with a high potential of exporting and receiving larvae around Mahé island.

UNIVERSITÉ CATHOLIQUE DE LOUVAIN
Faculté des bioingénieurs
Croix du Sud, 2 bte L7.05.01, 1348 Louvain-la-Neuve, Belgique | **www.uclouvain.be/agro**